

## Suspended sediment properties in the Lower Mekong River, from fluvial to estuarine environments

Le, Hoang-Anh; Gratiot, Nicolas; Santini, William; Ribolzi, Olivier; Tran, Duc ; Meriaux, Xavier ; Deleersnijder, Eric; Soares-Frazão, Sandra

**DOI**

[10.1016/j.ecss.2019.106522](https://doi.org/10.1016/j.ecss.2019.106522)

**Publication date**

2020

**Document Version**

Accepted author manuscript

**Published in**

Estuarine, Coastal and Shelf Science

**Citation (APA)**

Le, H.-A., Gratiot, N., Santini, W., Ribolzi, O., Tran, D., Meriaux, X., Deleersnijder, E., & Soares-Frazão, S. (2020). Suspended sediment properties in the Lower Mekong River, from fluvial to estuarine environments. *Estuarine, Coastal and Shelf Science*, 233, 1-14. Article 106522. <https://doi.org/10.1016/j.ecss.2019.106522>

**Important note**

To cite this publication, please use the final published version (if applicable). Please check the document version above.

**Copyright**

Other than for strictly personal use, it is not permitted to download, forward or distribute the text or part of it, without the consent of the author(s) and/or copyright holder(s), unless the work is under an open content license such as Creative Commons.

**Takedown policy**

Please contact us and provide details if you believe this document breaches copyrights. We will remove access to the work immediately and investigate your claim.

# 1 Suspended sediment properties in the Lower Mekong River, from fluvial to 2 estuarine environments

3  
4 **Hoang-Anh Le** <sup>1,2</sup>, **Nicolas Gratiot** <sup>2,3,\*</sup>, **William Santini** <sup>4</sup>, **Olivier Ribolzi** <sup>4</sup>, **Duc Tran** <sup>5</sup>,  
5 **Xavier Meriaux** <sup>6</sup>, and **Eric Deleersnijder** <sup>7,8</sup>, **Sandra Soares-Frazaõ** <sup>1</sup>

6  
7 <sup>1</sup> Civil and Environmental Engineering, Institute of Mechanics, Materials and Civil Engineering (IMMC),  
8 Université catholique de Louvain, Place du Levant 1, B-1348 Louvain – la – Neuve, Belgium

9 <sup>2</sup> Asian Research Center on Water (CARE-Rescif), Ho Chi Minh City University of Technology, Block B7, 268  
10 Ly Thuong Kiet Street, District 10, Ho Chi Minh City, Vietnam

11 <sup>3</sup> CNRS, IRD, IGE, Université Grenoble Alpes, F-38000 Grenoble, France

12 <sup>4</sup> Géosciences Environnement Toulouse (GET), Université de Toulouse, IRD, CNRS, UPS, Toulouse, France

13 <sup>5</sup> Faculty of Environment and Natural Resources, Ho Chi Minh City University of Technology, VNU-HCM,  
14 268 Ly Thuong Kiet, Ho Chi Minh City, Vietnam

15 <sup>6</sup> Université Littoral Côte d'Opale, Université Lille, CNRS, UMR 8187, LOG, Laboratoire d'Océanologie et de  
16 Géosciences, F 62930 Wimereux, France

17 <sup>7</sup> Université catholique de Louvain, Institute of Mechanics, Materials and Civil Engineering (IMMC) & Earth  
18 and Life Institute (ELI), 4 avenue Georges Lemaître, B-1348 Louvain-la-Neuve, Belgium

19 <sup>8</sup> Delft University of Technology, Delft Institute of Applied Mathematics (DIAM), Van Mourik Broekmanweg  
20 6, 2628XE Delft, The Netherlands

21  
22 \* Correspondence: [nicolas.gratiot@ird.fr](mailto:nicolas.gratiot@ird.fr); Tel.: +84-9-4129-4232

23  
24 **Abstract:** The Mekong river is one of the largest rivers in the world, which flows through  
25 six countries of Southeast Asia (China, Myanmar, Laos, Thailand, Cambodia and Vietnam).  
26 Its hydro-sedimentary regime is changing rapidly, as a consequence of a regional shift of  
27 land use (agriculture, road, etc.), damming, sand mining and climate changes, among others.  
28 This study assesses the behavior of particles transported in suspension in the Lower Mekong  
29 River (LMR), along approximately 1700 km from fluvial to estuarine environments.  
30 Suspended sediment properties were estimated, simultaneously with hydrodynamic  
31 conditions, during three field campaigns. In addition, further investigations were performed  
32 in the laboratory to assess the structures of particles (flocculated or not), their capacity to  
33 flocculate (and the impacts on siltation), under a wide range of sediment concentration (400  
34 to 4000 mg.L<sup>-1</sup>). This study confirms that suspended sediment transported in the LMR are  
35 predominantly (75 % by volume) flocculi (or freshly eroded soils aggregates), with median

60  
61  
62 36 aggregated particle size in the range 10 - 20  $\mu\text{m}$  and median settling velocity of the order of  
63 37 0.01 – 0.1  $\text{mm}\cdot\text{s}^{-1}$ . These flocculi are robust under the hydrodynamic conditions (turbulence  
64 38 and suspended sediment concentration – SSC) existing in the LMR. Laboratory  
65 39 investigations reveal the existence of a threshold sediment concentration (400  $\text{mg}\cdot\text{L}^{-1}$ ),  
66 40 beyond which flocculation and sedimentation increase of orders of magnitudes. Thus,  
67 41 concentration that exceeds this threshold might promote the formation of so-called fluid mud  
68 42 layers. Because of the nonlinear response of flocculation and sedimentation with SSC and  
69 43 considering the ongoing changes at a regional scale in the LMR, higher occurrence of fluid  
70 44 mud layers in the fluvial upstream waterbodies might be anticipated, and a lower occurrence  
71 45 in estuaries and alongshore where the concentration decrease. The geomorphology could be  
72 46 impacted, with an over-siltation in dams and an exacerbated erosion of the muddy-mangrove  
73 47 coast.

81  
82 48 **Keywords:** Mekong; LISST; SCAF; fluid mud layer; flocculation, settling velocity  
83  
84 49

## 85 86 50 **1. Introduction**

87  
88  
89 51 The Mekong river is the tenth longest river in the world with a length of 4909 km and has a  
90 52 basin area of 795,000  $\text{km}^2$ . Its mean annual discharge is approximately 475  $\text{km}^3$ , i.e. the sixth  
91 53 largest in the world. The river originates from the Tibetan Plateau (China) with an elevation of  
92 54 more than 5000 m above sea level (a.s.l.); then, the river flows through a variety of  
93 55 geomorphological and climatic systems and ends in the fertile delta of Vietnam (55,000  $\text{km}^2$ ),  
94 56 before discharging into the South East Sea of Vietnam (Mekong River Commission portal -  
95 57 MRC, [www.mrcmekong.org/](http://www.mrcmekong.org/)). Under human pressures and climate change, the river is facing  
96 58 many serious issues in link with changes in sediment dynamics. One of the most evident  
97 59 transformation is the construction of large hydropower dams in the upstream Mekong, which  
98 60 are modifying the hydrological cycle, and reducing the sediment discharge into the floodplain  
99 61 and estuaries at an alarming point (Schmitt et al., 2017). Sand mining in the delta is also a  
100 62 direct threat for the hydro-sedimentary budget. According to the literature, sediment flux has  
101 63 already decreased by almost five fold over 35 years, from about 160 mill.  $\text{tons}\cdot\text{year}^{-1}$  in 1983  
102 64 (Milliman et al., 1983) to  $87.4 \pm 28.7$  mill.  $\text{tons}\cdot\text{year}^{-1}$  in 2005 (Darby et al., 2016 and Schmitt  
103 65 et al., 2017) and  $40 \pm 20$  mill.  $\text{tons}\cdot\text{year}^{-1}$  in 2015 - 2016 (Thi Ha et al., 2018).  
104  
105  
106  
107  
108  
109  
110  
111  
112  
113  
114  
115  
116  
117  
118

119  
120  
121  
122  
123  
124  
125  
126  
127  
128  
129  
130  
131  
132  
133  
134  
135  
136  
137  
138  
139  
140  
141  
142  
143  
144  
145  
146  
147  
148  
149  
150  
151  
152  
153  
154  
155  
156  
157  
158  
159  
160  
161  
162  
163  
164  
165  
166  
167  
168  
169  
170  
171  
172  
173  
174  
175  
176  
177

66 Sand mining, trapping by dams, and the resulting reduction of sediment flux are undoubtedly  
67 corroborated with some changes in the nature (and populations) of particles transported. Some  
68 expected consequences in geomorphology, floodplain fertility and pollutant dynamics are  
69 already evoked (Kondolf et al., 2018), but need to be better studied. Previous studies  
70 conducted in the LMR indicated that the upper fluvial section was dominated by two particles  
71 size populations: silts, with a diameter of 10 - 20  $\mu\text{m}$ ; and sands, with a diameter of 63 - 200  
72  $\mu\text{m}$ , accounting for 78 % and 22 % of the total particle load, respectively (Peteuil et al., 2014).  
73 Downstream, in the estuary, flocculated fine particles dominate. The observed floc size,  
74 reported in the literature, was 30 - 40  $\mu\text{m}$ , constituting 60 - 80 % of the total sediment load in  
75 high flow season. However, in the low flow season, the floc size increased to 50 - 200  $\mu\text{m}$ ,  
76 accounting for 70 - 80 % of the total volume (Wolanski et al., 1996 and Wolanski et al.,  
77 1998). This observed variability of sediment properties reflects a direct adjustment of physical  
78 properties along streams, which operates at microscopic scales (flocculation, sedimentation  
79 and erosion), in link with hydrodynamic conditions and their seasonal variations. The  
80 different origins, together with different physicochemical and biological conditions between  
81 the sites, cause difficulties in interpreting the results.

82 Particle size, settling velocity and their spatio-temporal evolution through flocculation, are  
83 fundamental properties that need to be estimated to assess sediment transport and deposition  
84 processes in space and time (Manning et al., 2011a; Winterwerp, 2002). This is particularly  
85 true in the case of mud/sand mixtures, where complex interactions occur and need to be  
86 characterized for a realistic understanding of sediment dynamics (Manning et al., 2010).  
87 Conceptually, flocculation develops from primary particles into hierarchical structures,  
88 namely flocculi, microflocs and macroflocs. Primary particles mainly consist of fine particles  
89 with sizes of 1 - 6  $\mu\text{m}$ , and can be organic or inorganic. They aggregate to form 1<sup>st</sup> order  
90 structures, so-called flocculi, with diameters of the order of 6 - 50  $\mu\text{m}$ . They are usually  
91 hardly broken down into primary particles, even at the highest turbulent shear modulus  
92 experienced by particles in large rivers. Thus, it is generally considered that flocculi are a  
93 major component of sediment dynamics. Microflocs form the 2<sup>nd</sup> order of aggregation. They  
94 include primary particles and flocculi and have sizes of 50 - 200  $\mu\text{m}$ . Finally, macroflocs are  
95 the largest particle structures. They are loose structures with a wide size distribution, ranging  
96 from hundreds to thousands of micrometers (Lee et al., 2012 and Fettweis et al., 2006). Flocs  
97 (micro and macro) are generally fragile structures, easily broken down when passing through  
98 high turbulent shear modulus (Manning et al., 2011a).

178  
179  
180  
181  
182  
183  
184  
185  
186  
187  
188  
189  
190  
191  
192  
193  
194  
195  
196  
197  
198  
199  
200  
201  
202  
203  
204  
205  
206  
207  
208  
209  
210  
211  
212  
213  
214  
215  
216  
217  
218  
219  
220  
221  
222  
223  
224  
225  
226  
227  
228  
229  
230  
231  
232  
233  
234  
235  
236

99 Flocculation at microscopic scale, as some hydro-sedimentary and geomorphological impacts  
100 at scales of river reaches, estuaries and deltas, in particular because it promotes the formation  
101 of fluid mud layers. Fluid mud is defined as a mixture of high-concentrated fine sediments  
102 with water (Bachmann et al., 2005). It is generated by liquefaction of cohesive sediment beds  
103 by waves or by an imbalance between settling and eddy diffusion near the bed, or by the  
104 convergence of sediment fluxes from upstream and downstream. In energetic environments,  
105 large particles such as sand are also found in fluid mud samples, but the portion is less than  
106 few percent (McAnally et al., 2007). Fluid mud masses may be advected over large distances  
107 horizontally without losing their coherent nature or internal chemical properties; and its  
108 horizontal convergence may often be a key mechanism of their accumulation (McAnally et  
109 al., 2007). Thus, fluid mud in thin layers is considered as an intermediate stage of deposition  
110 (before formation of consolidated bed layers) or bed erosion (under entrainment process by  
111 fluidization (McAnally et al., 2007). Its thickness varies from few centimeters to meters  
112 (Sottolichio et al., 2011; Azhikodan et al., 2018).

113 The occurrence of fluid mud is commonly observed in quiescent environments such as lakes  
114 and reservoirs (Mehta et al., 1991; McAnally et al., 2007) or in the Estuarine Turbidity  
115 Maximum zones (ETM) (Uncle et al., 2006; Winterwerp et al., 2011; Azhikodan et al., 2018)  
116 such as estuaries, navigation channels, harbour basins or along muddy coasts all over the  
117 world (Bachmann et al., 2005; Schelske et al., 2006; Gratiot et al. 2007; Toorman et al. 2018).  
118 The turbidity maximum zone is often created by resuspension from the bed during parts of the  
119 tidal cycle and shows a significant drag reduction at high SSC concentration gradient (Dyer et  
120 al., 2002a and Dyer et al., 2002b). However it has been poorly studied and reported in the  
121 literature dedicated to the LMR (Wolanski et al., 1998, Xue et al., 2010) and received some  
122 more interest recently (Gugliotta et al., 2019; Nittrouer et al., 2017; Gratiot et al., 2017).

123 This study originally combines in situ measurements and laboratory investigations to examine  
124 the physics of particles (especially flocculation properties, measured with new patented  
125 equipment developed by SCAF®) and to understand transport/deposition processes in the  
126 LMR. Sampling and analyses are performed in three contrasted environments: an upper  
127 fluvial reach in Laos (Fig. 1b), a lacustrine environment in Cambodia (Fig. 1c) and an  
128 estuarine environment in Vietnam (Fig. 1d). The same methodology was applied for these  
129 three contrasted environments (upstream river, lake and estuary). Results obtained allow for  
130 answering and discussing the following points:

- 237  
238  
239 131 • Are suspended sediment flocculated or not (percentages of cohesive versus non-  
240 132 cohesive particles transported in suspension)?  
241  
242  
243 133 • If yes, are floc populations stable from upstream to downstream and/or highly  
244 134 dependent on hydrodynamic conditions (SSC, turbulence, salinity)?  
245  
246  
247 135 • Are suspended sediment predominantly transported as washload (single path with no  
248 136 bed interactions), or does it experience successive phases of deposition and erosion?  
249  
250  
251 137 • How much SSC increase can modify flocculation, sedimentation and how much this  
252 138 could contribute to the formation of fluid mud layers and, finally, modify the  
253 139 geomorphology of the LMR?  
254  
255  
256

257 140 By answering to the four questions above, the paper proposes a better understanding of the  
258 141 physical properties of sediment and their transportation modes along the Lower Mekong  
259 142 River. Because flocculation and fluid mud layers are playing an important role in the dynamic  
260 143 of the Mekong Delta, this information will facilitate the implementation of integrated tools,  
261 144 such as ecological/geomorphological models, to go through a better management of large  
262 145 scale hydrosystems.  
263  
264  
265  
266  
267

## 268 146 **2. Study areas and Methods**

### 269 147 *2.1. Study area*

270  
271  
272  
273 148 Field investigations have been conducted at three locations of the LMR, assumed to be  
274 149 representative of river morphological units, from the upper fluvial environment to the  
275 150 lacustrine and the estuarine environments (Fig. 1a).  
276  
277  
278

#### 279 151 *2.1.1. Fluvial environment*

280  
281 152 The upper fluvial reach considered is located at the level of Luang Prabang city, Laos  
282 153 (Fig.1b). It is situated on a long stem at the confluence of the Mekong and Nam Khan rivers, a  
283 154 tributary of the Mekong. Its altitude is approximately 300 m a.s.l. This area is covered with  
284 155 steep hillsides and has been experiencing drastic land use changes, predominantly leading to  
285 156 erosion, since the last decades (Ribolzi et al., 2017). At Luang Prabang, the Mekong river  
286 157 section is already wide, with width of 600 - 700 m. However, when passing through gorges,  
287 158 the channel becomes swiftly narrow, approximately 100 m wide, and bounded by limestone  
288  
289  
290  
291  
292  
293  
294  
295

296  
297  
298 159 pavement. The channel has a median depth of around 10 m, with maximum depth of  
299  
300 160 approximately 30 m (Gupta et al., 2007).

301 161 The field survey was conducted for 8 days, from 26 June to 2 July 2017, at the beginning of  
302  
303 162 the wet season. There were neither extreme floods nor low water situations, thus the  
304  
305 163 hydrodynamic conditions were suitable for sampling and analysing a typical (median)  
306  
307 164 suspended sediment distribution in the river. Twenty-seven samples were taken in the main  
308  
309 165 Mekong river and its tributaries (Nam Ou, Nam Suang and Nam Khan tributaries). During the  
310  
311 166 survey, hydro-sedimentary conditions were also characterized on two cross-sections with  
312  
313 167 distances of approximately 20 km (Fig. 1a, see section 2.2.3). For each location, samples were  
314  
315 168 collected in three vertical profiles (left bank – V1, middle bank – V2 and right bank – V3). In  
316  
317 170 each vertical profile, 3 litres of water sample were taken at various depths (0.1 h, 0.4 h, 0.7 h  
318  
319 and 0.9 h, h being total water depth).

### 318 171 2.1.2. Lacustrine environment

320  
321 172 With volume of 1.8 – 58.3 billion m<sup>3</sup>, the Tonle Sap lake is the largest freshwater source in  
322  
323 173 Southeast Asia (Kummu et al., 2014). It is located in the Cambodian floodplain (Fig. 1c) and  
324  
325 174 comprises a permanent waterbody, twelve tributaries, extensive floodplains and the Tonle Sap  
326  
327 175 river linking the lake to the Mekong river (Kummu et al., 2014). At the confluence, the river  
328  
329 176 splits into the Bassac river (Hau river) in the West and the Mekong river (Tien river) in the  
330  
331 177 East. The Tonle Sap system has strong and original hydrodynamic relationships with the  
332  
333 178 Mekong mainstream (Kummu et al., 2008). During the wet season, flooding from the Mekong  
334  
335 179 river causes a reverse flow direction, into the Tonle Sap lake. The lake area then increases  
336  
337 180 from 2500 km<sup>2</sup> to approximately 15000 km<sup>2</sup>, while the depth rises from 1 to 9 m. At the  
338  
339 181 opposite, the slow release of floodwaters from the lake during the dry season is a very  
340  
341 182 important water source to sustain the river discharge of the Mekong delta (Hai et al., 2008). In  
342  
343 183 this specific paper, we focus on the physics of particles. The field survey was performed for 9  
344  
345 184 days from 13 October to 21 October 2018, during high flow season. The material used is  
346  
347 185 freshly deposited sediment, collected near the Mekong river tributaries, after a flood season at  
348  
349 186 the bottom layer.

### 345 187 2.1.3. Estuarine environment

347  
348 188 The Mekong delta (MD) is situated at the most Southeast part of the LMR (Fig. 1d). It covers  
349  
350 189 approximately 55,000 km<sup>2</sup> (Balica et al., 2014), extending from the Cambodia - Vietnam  
351  
352 190 border to the Gulf of Thailand and the East Sea of Vietnam (Tran et al., 2018). Together with  
353  
354

355  
356  
357  
358  
359  
360  
361  
362  
363  
364  
365  
366  
367  
368  
369  
370  
371  
372  
373  
374  
375  
376  
377  
378  
379  
380  
381  
382  
383  
384  
385  
386  
387  
388  
389  
390  
391  
392  
393  
394  
395  
396  
397  
398  
399  
400  
401  
402  
403  
404  
405  
406  
407  
408  
409  
410  
411  
412  
413

191 the Mekong river and the Bassac river, it separates into eight tributaries (Hung et al., 2014)  
192 before discharging into the East Sea (Wolanski et al., 1996 and Xing et al., 2017). At the  
193 interface between land and the sea, the estuary is strongly impacted by both flooding from  
194 upstream and the tidal flows, as well as wave forcing (Gugliotta et al., 2019).

195 Three surveys with contrasted seasonal conditions were conducted in the Song Hau estuary  
196 (as part of the Lower Mekong Delta Coastal Zone project), in December 2015, March and  
197 October 2016. During these surveys, three cross-sections (upstream - T1, middle - T2,  
198 downstream - T3), with distances of 10 and 15 km, respectively, were chosen to monitor and  
199 assess the impact of saline water intrusion on flocculation (Fig. 1d and sketch of Fig.6). At  
200 each location, samples were taken in three vertical profiles. In total, 104 samples with volume  
201 of 5 litres per sample were collected to investigate the spatio-temporal dynamics of suspended  
202 sediment for contrasted sediment concentration (SSC) and turbulent levels.



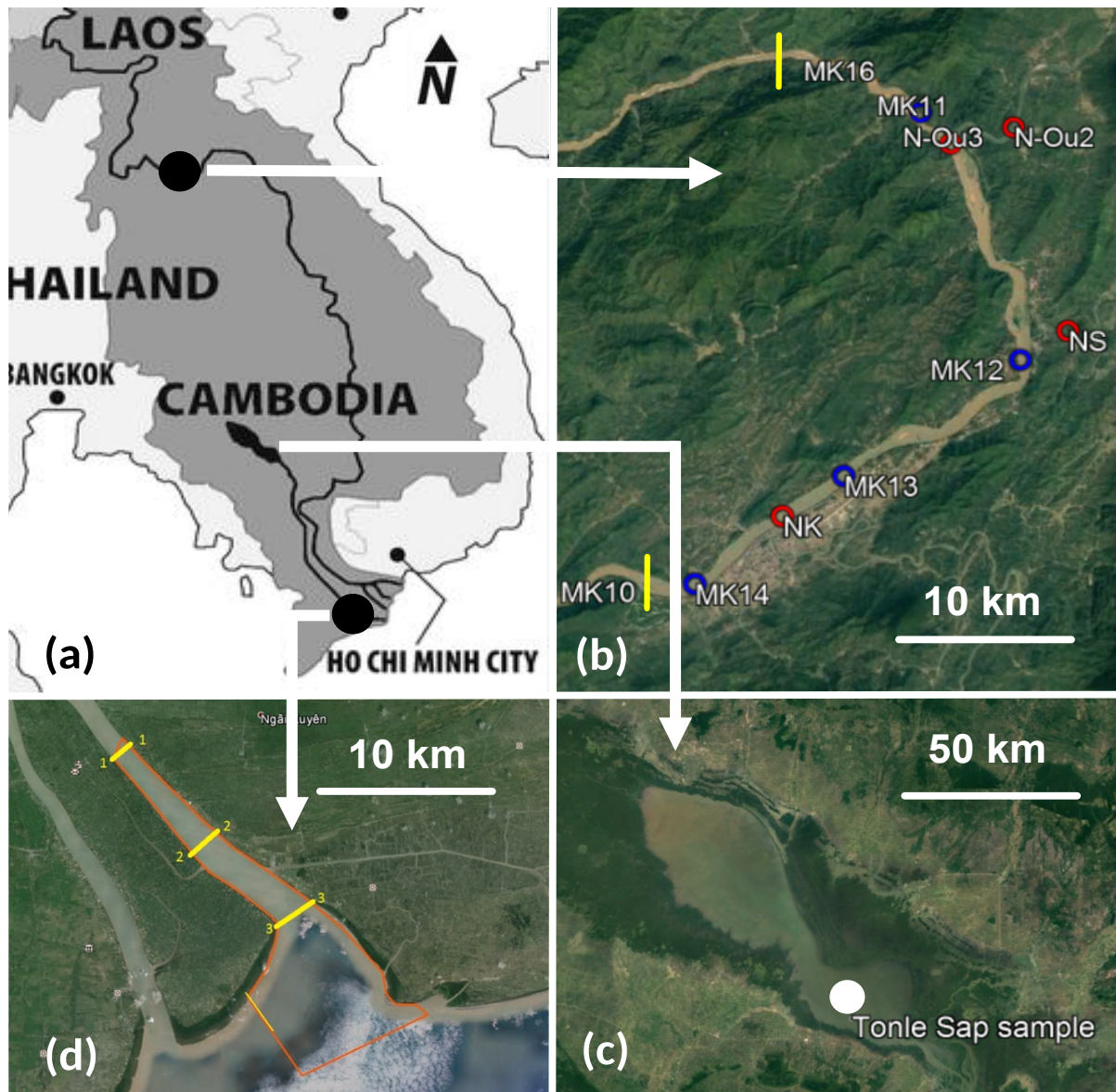


**Fig. 1.** Domains of interest [a] (Smardon et al., 2009). Sampling sites and locations in fluvial (Luang Prabang, Laos with blue dots reporting samples in main stream, red dots reporting samples in tributaries and yellow segments reporting cross-sections [b]), lacustrine environment (Tonle Sap floodplain, Cambodia with white dots showing the sampling location [c]), and estuarine environment (Song Hau estuary, Vietnam with yellow segments reporting cross-sections and red lines showing the local domain [d]).

*2.2. Methods*

The suspension regime of the sediments transported in a flow strongly depends on interactions between hydrodynamics, particle size, density and settling velocity. Thus, the understanding of particle size distribution (PSD) of suspended particulate matter (SPM) is one of prerequisites to properly simulate sediment dynamics (Fennessy et al., 1994). This study

473  
474  
475  
476  
477  
478  
479  
480  
481  
482  
483  
484  
485  
486  
487  
488  
489  
490  
491  
492  
493  
494  
495  
496  
497  
498  
499  
500  
501  
502  
503  
504  
505  
506  
507  
508  
509  
510  
511  
512  
513  
514  
515  
516  
517  
518  
519  
520  
521  
522  
523  
524  
525  
526  
527  
528  
529  
530  
531

215 originally proposes a direct estimation of settling velocity and flocculation with the patented  
216 SCAF instrument (System for the Characterization of Aggregates and Floccs, Gratiot et al.  
217 2015).

218 The five sections hereinafter describe the methodology adopted to measure the physical  
219 properties of suspended sediment and evaluate its transport dynamics. The instruments at our  
220 disposal are particularly relevant to estimate both particle size and settling velocity, but it was  
221 not possible to measure directly the density of floccs, which may be seen as a limitation.

#### 222 2.2.1. A portable mixing tank device to reproduce natural inflow turbulent conditions

223 To measure PSD under turbulent conditions close to the ones experienced by natural rivers, 2  
224 litres of water samples were introduced into a portable rectangular-base mixing jar tank (with  
225 diameter of 11.5 x 11.5 x 15 cm), and then mixed with an impeller for thirty minutes. Since  
226 the work of Gratiot and Manning (2004), this mixing duration is assumed to ensure a good  
227 homogenization of the fluid mud mixture, and a dynamic equilibrium between the rate of  
228 flocculation and breakage. Some details on the experimental set-up can be found in Gratiot et  
229 al. (2017). During preliminary experiments, an Acoustic Doppler Velocity Profiler (Nortek  
230 Vectrino2) was immersed in the mixing tank filled with clear water, in order to measure  
231 the 3D turbulent field of velocity and deduce the mean turbulent energy dissipation rate  $G$  ( $s^{-1}$ ).  
232 With a rotation speed of 100 rpm,  $G$  was about  $44 s^{-1}$ , which corresponds to high shear rate  
233 conditions, such as observed near bottom in natural rivers and estuaries (Gratiot et al., 2017).  
234 For further details on the mixing tank device, the reader can refer to Gratiot et al. (2017,  
235 supplementary information).

#### 236 2.2.2. PSD measurements and characterization of the particle-classes/population/group?

237 To characterize the different populations of particles, the terminology of Lee et al. (2012) is  
238 used. It is based on four classes, namely primary particles, flocculi, microflocs and macroflocs  
239 (as mentioned in the Introduction section). We utilize the LISST-Portable XR instrument to  
240 measure sediment particle sizes during mixing. The operational principle of the LISST-  
241 Portable XR is based on laser light scattering (or laser diffraction). This instrument provides  
242 the logarithmical PSDs over 44-size bands in the ranges of particle size from 0.35 to 500  $\mu m$   
243 by using the Fraunhofer approximation or the exact Lorenz-Mie theory. The volumic  
244 concentration is in micro-litre/litre ( $\mu L.L^{-1}$ ), corresponding to sediment concentration of 30 -  
245 1900  $mg.L^{-1}$  in the chamber of measurement. Each spectrum shows independent semi-log  
246 distributions of sub-populations, that were characterized by their mean particle size  $D_f$ , their

532  
533  
534  
535  
536  
537  
538  
539  
540  
541  
542  
543  
544  
545  
546  
547  
548  
549  
550  
551  
552  
553  
554  
555  
556  
557  
558  
559  
560  
561  
562  
563  
564  
565  
566  
567  
568  
569  
570  
571  
572  
573  
574  
575  
576  
577  
578  
579  
580  
581  
582  
583  
584  
585  
586  
587  
588  
589  
590

247 standard deviation  $\sigma_{Df}$  and their relative volumetric concentration. The operating range of  
248 optical transmission recommended by LISST-Portable XR is 75 - 95 %. For optical  
249 transmission lower than 75 %, multiple-scattering can bias the signal and lead to an  
250 underestimation of the size distribution.

251 This device has been utilized successfully in many contrasted environments, such as the  
252 Saigon - Dong Nai rivers, Vietnam (Nguyen et al., 2019), a hydropower plant in Malaysia  
253 (Azrulhisham et al., 2018), Northern French Alps (Antoine et al., 2015) and Philadelphia  
254 (Windt et al., 2017), among others.

255 It is worth noting that many other techniques exist to measure PSD, particularly video-based  
256 techniques, such as the immersed INSSEV instrument (Fennessy et al., 1994) or the LabFlocs  
257 portable video system (Manning et al., 2007). All methods have advantages and  
258 disadvantages, so that a combination of different techniques is probably the best efficient.

259  
260 For describing PSDs of primary particles, flocculi, microflocs and macroflocs, we apply a  
261 mathematical function to separate the signal into four log-normal distribution (Mikkelsen et  
262 al., 2006). Such post processing is also useful to prevent misinterpretation, resulting from air  
263 bubbles and other artefacts that can be observed in the raw particle size spectrum (Sequoia,  
264 2016).

265 In this study, the PSD of each sample was measured in two steps, before and after two  
266 minutes of sonication, for a mechanical particle breakage under acoustic waves. Hence, it is  
267 possible to assess the proportion of sand and flocs because large-size particles built by smaller  
268 cohesive particles (silt or clay) are, at least partially, dispersed by sonication (Gratiot et al.,  
269 2017) while the sand particles are indivisible and then maintain a constant diameter after  
270 sonication.

### 271 2.2.3. Characterization of the settling and flocculation regimes

272 Depending on SSC, three settling regimes can be observed for natural sediment in aquatic  
273 environment (Van Leussen, 1994), namely (1) free settling, (2) flocculation and (3) hindered  
274 regimes. For the lowest SSC, flocculation is weak and particles are settling almost  
275 independently from each other (free settling regime). Particle settling velocity can then be  
276 broadly estimated by the Stokes' law or derived laws as the sum of individual particles  
277 settling down (Stokes, 1857; Winterwerp, 2002). The flocculation settling regime occurs with  
278 midrange of SSC (tens to hundreds of  $\text{mg.L}^{-1}$ ). The settling velocity of cohesive and mixed  
279 fine-grained sediments then becomes more complex because it is influenced by both particle

591  
592  
593 280 interactions and individual properties (Manning et al., 2010), as well as turbulent shear  
594  
595 281 (Winterwerp, 2002; Manning et al, 2011a). Flocculation is promoted, which results in larger  
596  
597 282 particle sizes and higher settling velocities (Droppo et al., 2005). The hindered settling regime  
598  
599 283 occurs at very high SSC (several grams per litre or more), and settling mostly occurs by mass,  
600  
601 284 depending on the cohesion and suspension concentration (Camenen and Van Bang, 2011; Van  
602  
603 285 and Van Bang, 2013).

604 286 To assess the settling velocity  $w_s$  (m.s<sup>-1</sup>) (and flocculation) for all these regimes in natural  
605  
606 287 environment, we used the System for the Characterization of Aggregates and Flocs (SCAF), a  
607  
608 288 recently patented instrument (Gratiot et al., 2015) that was successfully applied in some recent  
609  
610 289 researches (Wendling et al., 2015, Gratiot et al., 2017, Legout et al., 2018, Nguyen et al.,  
611  
612 290 2019). This instrument is a glass settling column with dimension of 20 cm high and 3.5 cm in  
613  
614 291 diameter, equipped with 16 infrared ( $\lambda = 980$  nm) emitters and 16 diametrically opposed  
615  
616 292 photo-sensors measuring at a frequency of 210 Hz. SCAF instrument measures the light  
617  
618 293 attenuation in the settling tube with depth and time during the deposition of particles (Gratiot  
619  
620 294 et al., 2015). Sensors are located every 1 cm down the column with the lower sensor located at  
621  
622 295 1 cm above the bottom of the column. Measurements taken in the eight upper centimeters of  
623  
624 296 the SCAF settling tube provided an estimate of flocs settling velocity under quiescent  
625  
626 297 conditions, denoted  $w_{s,q}$  (m.s<sup>-1</sup>) while measurements realized in the eight centimetres near the  
627  
628 298 bottom of the settling tube provided an estimation of flocs settling velocity after flocculation  
629  
630 299 by differential settling under settling dominated conditions, this latter velocity being reported  
631  
632 300 as  $w_{s,\neq}$  (Wendling et al., 2015). In the case of non-cohesive particles, such as sand or silt, or  
633  
634 301 clay particles with deflocculant, the settling velocity does not change during settling;  $w_{s,q}$  and  
635  
636 302  $w_{s,\neq}$  are similar and the flocculation index  $FI = (w_{s,\neq} - w_{s,q}) / w_{s,q}$  is close to zero (Wendling et  
637  
638 303 al., 2015). As SCAF instrument is based on by mass sedimentation of a fluid mud mixture in a  
639  
640 304 settling tube, it is inherently affected by the shape, density and compositions of all particles  
641  
642 305 presented in the sample.

#### 636 306 2.2.4. Other hydrodynamic measurements

639 307 Complementary measurements were performed during field surveys. An Acoustic Doppler  
640  
641 308 Current Profiler (ADCP), an Hydrolab probe (a multi-parameter probe measuring in-situ  
642  
643 309 water quality parameters), SSC samplers and a EUTECH turbidimeter were used to  
644  
645 310 characterize the water flow in the cross-sections, suspended solid concentration and physical  
646  
647 311 parameters such as turbidity, temperature, pH, ORD, EC, salinity, etc. An YSI multi-

parameter probe (Water Quality Sampling and Monitoring Meters and Instruments) was also used to check the average values of the measured physical parameters.

### 2.2.5 Characterization of the suspension regime

In order to characterize the suspension regime, the non-dimensional Rouse number (Rouse, 1937), which express the balance between the upward turbulence forces ( $u_*$ ) lifting the particles and the gravity forces applied ( $w_s$ ) on the same particles in a river stream, was calculated for each flow condition encountered. The Rouse number is calculated as following:

$$R_o = \frac{w_s}{\beta \kappa u_*} \quad (1)$$

where the settling velocity  $w_s$  is inferred from the SCAF results (Fig. 5), or calculated by the Stokes' Law from the PSD measurements.  $\kappa$  is the von Kármán constant, taken equal to 0.41. The constant of proportionality  $\beta$  is the ratio of sediment to eddy diffusivity, describing the diffusion patterns of a fluid particle and a sediment particle. In water environment, it is often assumed that eddy viscosity is equal to eddy diffusivity, thus value  $\beta$  is typically hypothesised to be one (Rijn, 1984; Farrell and Sherman, 2013).  $u_*$  ( $\text{m.s}^{-1}$ ) is shear velocity. In the fluvial and estuarine environments, the shear velocity  $u_*$  was computed by using the ADCP, with the assumption that the velocity profiles follow the logarithmic inner-law (so-called "Law of the Wall") (Sime et al., 2007; Santini et al., 2019, Eidam et al., 2017). In the lacustrine environment,  $u_*$  was computed from 2D hydrodynamic simulation results by the Second-generation Louvain-la-Neuve Ice-ocean Model (SLIM, <https://www.slim-ocean.be/>).

The application of Eq.1 to characterize the suspension regime is relevant, but we should underline that uncertainties can be high, as both  $w_s$  and  $u_*$  are hardly estimate in the field.

## 3. Results

### 3.1. Particle size distribution (PSD)

The PSD of all samples are gathered in a triangle sketch in Fig. 2. Before sonication, most of the particles are flocculi with an average contribution percentage of 46 %, 78 % and 78 %, for fluvial, lacustrine and estuarine environments, respectively (Fig. 2a). After sonication, the PSD displayed an increased number of primary particle class for all samples (51 %, 67 % and

709  
710  
711 339 32 %, respectively), while it witnessed the reduction in the percentage of flocculi and flocs  
712  
713 340 (Fig. 2b). This figure also shows a wider diversity of particle sizes in the Mekong estuary  
714  
715 341 (blue circles and squares) than in the lacustrine and the fluvial environments (yellow and red  
716 342 circles, respectively). It illustrates that estuaries are complex and changing environments,  
717  
718 343 which mix both fluvial and coastal water (see the sketch in Fig.6 and the corresponding  
719 344 discussion section). In the case of the Mekong estuaries zone, sediment transport and  
720  
721 345 deposition is strongly affected by fluvial inflow, tidal currents, but also resuspension of  
722  
723 346 particles by wind-induced current, waves and coastal oceanic currents (Gugliotta et al., 2019;  
724 347 Marchesiello et al., 2019).  
725  
726  
727  
728  
729  
730  
731  
732  
733  
734  
735  
736  
737  
738  
739  
740  
741  
742  
743  
744  
745  
746  
747  
748  
749  
750  
751  
752  
753  
754  
755  
756  
757  
758  
759  
760  
761  
762  
763  
764  
765  
766  
767

768  
769  
770  
771  
772  
773  
774  
775  
776  
777  
778  
779  
780  
781  
782  
783  
784  
785  
786  
787  
788  
789  
348  
791  
792  
349  
793  
794  
795  
796  
797  
798  
799  
800  
801  
802  
803  
804  
805  
806  
807  
808

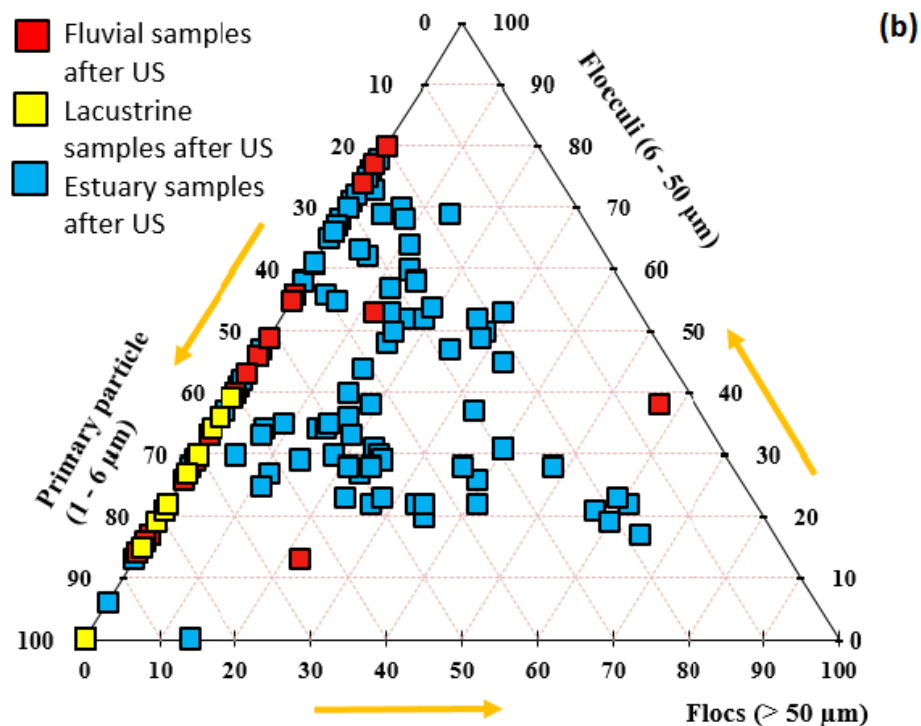
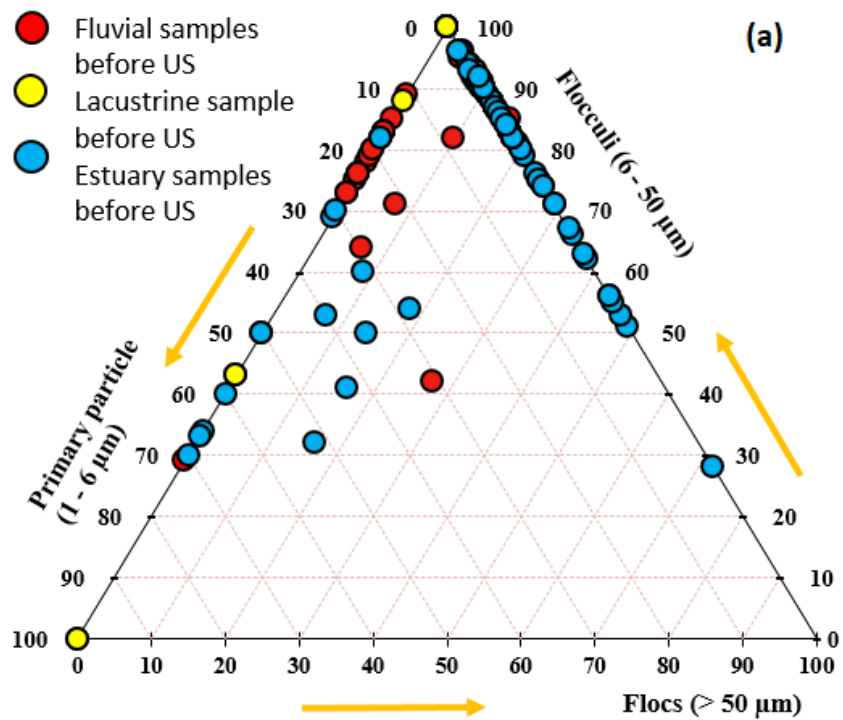
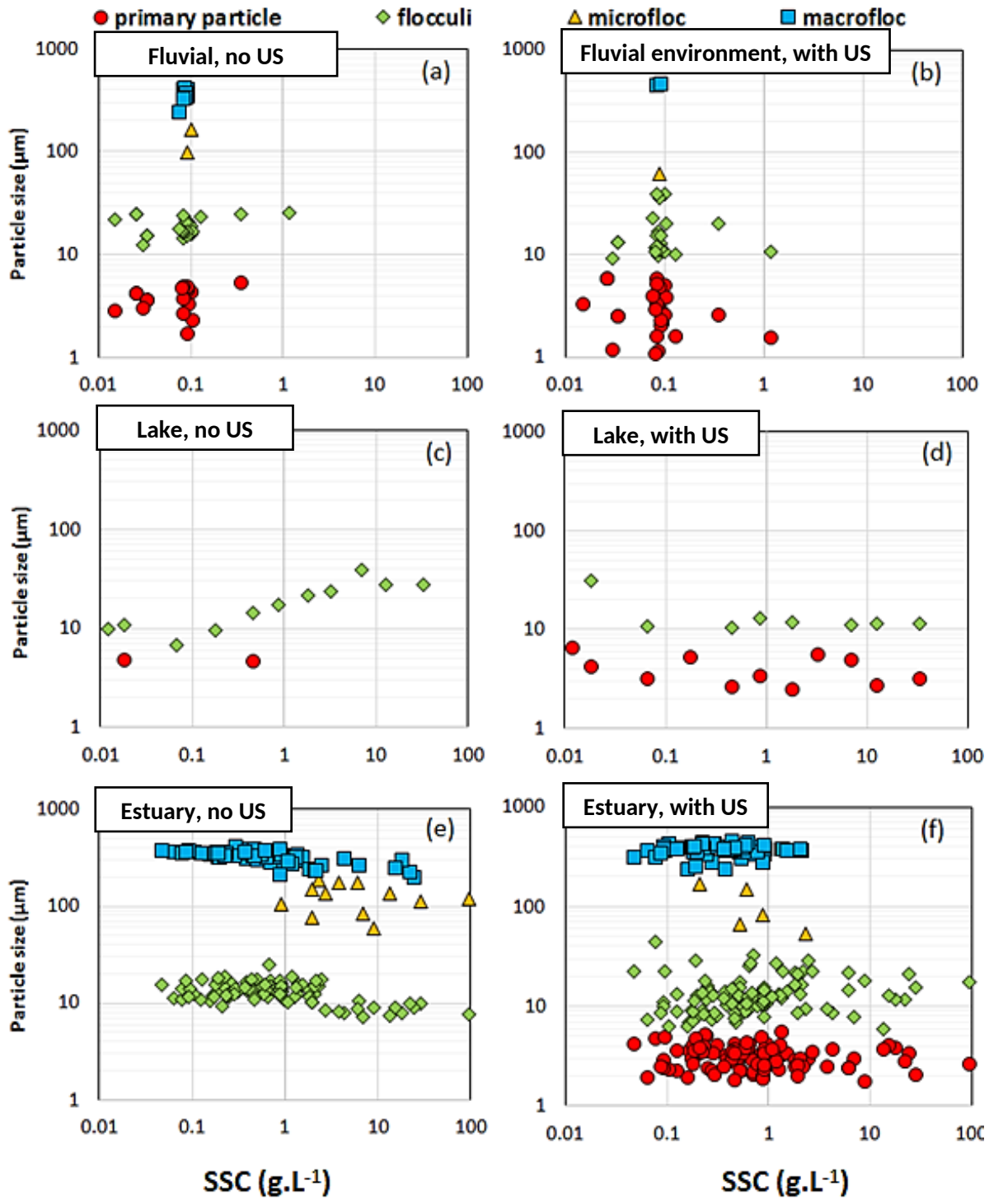


**Fig. 2.** Triangulars of PSD in upper parts and estuary analyzed (a) before and (b) after sonication

809  
810  
811  
812  
813  
814  
815  
816  
817  
818  
819  
820  
821  
822  
823  
824  
825  
826  
827  
828  
829  
830  
831  
832  
833  
834  
835  
836  
837  
838  
839  
840  
841  
842  
843  
844  
845  
846  
847  
848  
849  
850  
851  
852  
853  
854  
855  
856  
857  
858  
859  
860  
861  
862  
863  
864  
865  
866  
867

350 3.2. Suspended sediment versus hydrodynamic conditions

351 Fig. 3 aims at highlighting the role played by SSC on flocculation of particles. This figure  
352 gathers both data collected in the field and in the laboratory, before and after sonication.



353  
354 **Fig. 3.** Variation of particle classes with SSC in fluvial environment, lacustrine environment  
355 and estuary before and after sonication



868  
869  
870 356 3.2.1. Particle size populations in the fluvial environment (Laos)  
871

872  
873 357 Fig. 3 (a) and Fig. 3 (b) present the PSD of particles populations sampled in the fluvial  
874 358 section. On average, the primary particles accounted for 37 % of all particle population (in  
875 359 volumetric concentration). The predominant population is flocculi, with a volume  
876 360 concentration of approximately 46 %. Microflocs and macroflocs were fewer and accounted  
877 361 for (only) 3 % and 14 % of the total volume, respectively. The macroflocs size reached a  
880 362 median diameter of 422  $\mu\text{m}$ . Fig. 3 (b) shows the PSD plot after sonication. The sonication  
882 363 broke up particles so that the percentage of primary particles increased (+14 %) to 51 % and  
883 364 flocculi decreased slightly (-5 %) to 41 %. The percentage of microflocs remains stable and  
885 365 small (approximately 2 %), and the percentage of macroflocs decreases by more than two  
887 366 folds (to approximately 6 %). These coarsest particles were not all broken up by sonication,  
888 367 which indicates the presence of sand. The samples issued from the tributaries had generally  
890 368 similar PSDs than the ones in the mainstream. After sonication, PSD of these samples still  
892 369 exhibits high values, with a maximum diameter of 347  $\mu\text{m}$ . It means that these water samples  
893 370 contains predominantly sand, which is in agreement with visual observations during field  
894 371 campaigns. A detailed examination of PSD before and after sonication confirmed that samples  
895 372 in fluvial environment consisted of both cohesive sediment and sand particles. These PSDs  
898 373 are in agreement with the results of Camenen et al. (2014).

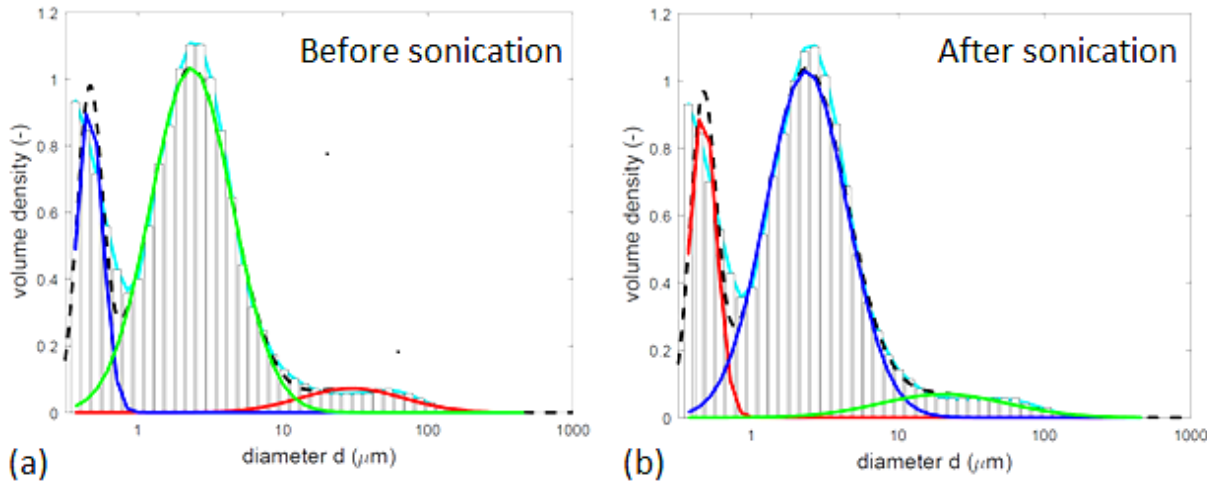
900  
901 374 3.2.2. Particle size populations in the lacustrine environment (Tonle Sap, Cambodia)  
902

903 375 In the lacustrine environment, only two particles classes (primary particles and flocculi,  
904 376 without flocs and no sands) appear. Before sonication (see Fig. 3c), the percentage of primary  
905 377 particles and flocculi accounts for 22 % and 78 %, respectively. After sonication (see Fig. 3d),  
907 378 these percentages reverse with a predominance of primary particle (67 %) and a simultaneous  
909 379 decrease of flocculi (33 %). The particle size in the lacustrine environment were smaller ( $7 \pm$   
911 380  $3 \mu\text{m}$ ) than in the fluvial part ( $18 \pm 5 \mu\text{m}$ ). Fig. 3c exhibits a clear rise (3 to 4 folds) of flocculi  
912 381 size with higher SSC, as a response of flocculation of primary particles (or colloids) on  
914 382 flocculi.

916  
917 383 Interestingly, colloids were observed in some samples taken in the Tonle Sap, with diameters  
918 384 of  $< 1 \mu\text{m}$  (see Fig 4). After 12 hours of deposition in the mixing tank at rest, the particles still  
919 385 in suspension were both colloids with diameter of approximately 0.45  $\mu\text{m}$ , which are  
920 386 consistence with a research conducted by Seah et al 2017, accounting for 21 %; primary  
921  
922  
923  
924  
925  
926

927  
928  
929  
930  
931  
932  
933  
934  
935  
936  
937  
938  
939  
940  
941  
942  
943  
944  
945  
946  
947  
948  
949  
950  
951  
952  
953  
954  
955  
956  
957  
958  
959  
960  
961  
962  
963  
964  
965  
966  
967  
968  
969  
970  
971  
972  
973  
974  
975  
976  
977  
978  
979  
980  
981  
982  
983  
984  
985

387 particle (73 %) and few flocculi (6 %). After sonication, the structure of sediments presents  
388 the same pattern (21 % of colloid, 72 % of primary particles and 7 % of flocculi). This can be  
389 explained by a stable mixture of this sediment classes, which are hardly broken down into  
390 smaller particles even after sonication. Colloids play an important role and act as “catalyzers”  
391 of the interaction between sediment and substances in the water such as substance dissolved  
392 matter, substance from precipitation, absorbed ions and organic matters (Wendling et al.,  
393 2015).



394  
395 **Fig 4.** PSD of a sample in the Tonle Sap before (a) and after sonication (b). The first peaks in  
396 two graphs show the appearance of colloids with diameter of < 1 μm.

### 397 3.2.3. Particle size populations in the estuarine environment (Song Hau river, Vietnam)

398 Fig 3 (e and f) display the PSD in the estuary versus SSC before and after sonication,  
399 respectively. Once again, flocculi is the dominant population of particles, with mean diameter  
400 of approximately 15 μm (in range of 8 - 20 μm), accounting for 80 % of total volume. Before  
401 sonication, only three classes of particle sizes exist in the estuarine samples, flocculi,  
402 microflocs and macroflocs. The prevailing fine silt population shows mean diameter of 7 –  
403 12.5 ± 10 % μm, that constituted 83 – 94 % of total volume. Diameters of coarser population  
404 were in the range of 112 – 310 ± 10 % μm. After sonication, particle size reduced  
405 significantly. A group of primary particles (red circles), which were completely absent from  
406 the PSDs before sonication, appears in almost all samples, which undoubtedly demonstrates  
407 the cohesive nature of sediments in the estuary. Due to breakage into smaller particles under  
408 turbulence shear, diameters of fine particles (primary particles and flocculi) reduce to 1.8 – 4  
409 ± 10 % μm and 6.3 – 12.2 ± 10 % μm, respectively while the size of coarse particle

986  
987  
988 410 (microflocs) falls to  $15 - 65 \pm 10 \%$   $\mu\text{m}$ . A population of sand particles (with diameter  $> 200$   
989 411  $\mu\text{m}$ ), not broken-up with/after sonication, is also evidenced.

### 992 412 3.3. *Settling velocity*

993  
994  
995 413 Fig. 5(a) shows the variation of suspended sediment settling velocity with SSC, measured  
996 414 directly with SCAF instrument. For the three aquatic environments, settling velocity rises with  
997  
998 415 SSC because of flocculation process. Even if there are only 5 SCAF samples in the fluvial  
999  
1000 416 environment, 9 samples in lacustrine environment, 19 samples in the estuary, the three curves  
1001 417 exhibit similar trends, which support the existence of free settling, flocculation and hindered  
1002  
1003 418 regimes, as previously depicted by Wendling et al. (2015).

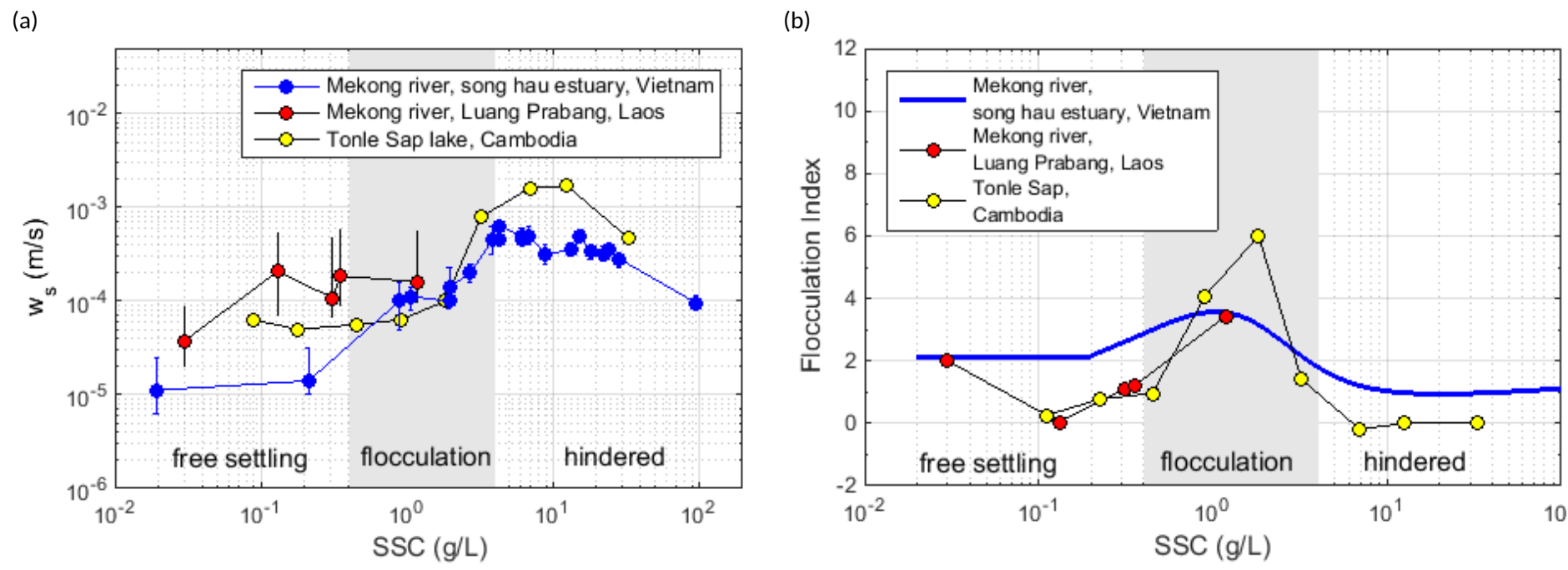
1004  
1005 419 The free settling regime is observed for the lowest SSC (tens of  $\text{mg.L}^{-1}$ ). Sediment settling  
1006  
1007 420 velocity measured in the fluvial, lacustrine and estuarine environments are of the same order  
1008  
1009 421 of magnitude, the mean settling velocities being approximately  $0.02 - 0.08 \text{ mm.s}^{-1}$  in the  
1010 422 fluvial section,  $0.05 - 0.06 \text{ mm.s}^{-1}$  in the lake, and  $0.01 - 0.02 \text{ mm.s}^{-1}$  in the estuary. The  
1011  
1012 423 widest range of settling velocities observed in the fluvial environment is probably the  
1013 424 fingerprinting of a wide variety of compact soil aggregates, freshly eroded from the  
1014  
1015 425 watershed, and not yet at equilibrium with the prevailing hydrodynamic conditions, as  
1016  
1017 426 reported conceptually by Droppo et al. (2015). In this free settling regime, particles settle  
1018 427 almost independently, the interaction between particles is poor, which is reflected by a  
1019  
1020 428 moderate flocculation index (FI lower than 2) in all SCAF measurements (in Fig. 5, right  
1021 429 panel). Flocculation predominates in the range of  $0.4 - 4 \text{ g.L}^{-1}$ , thus the settling velocities of  
1022  
1023 430 fluvial, lacustrine and estuarine sediments rise up to  $0.2 \text{ mm s}^{-1}$ ,  $0.1 - 2 \text{ mm.s}^{-1}$  and  $0.03 - 0.8$   
1024  
1025 431  $\text{mm.s}^{-1}$ , respectively.

1026  
1027 432 In the lacustrine environment, a significant rise of settling velocity is found with higher SSC.  
1028  
1029 433 The SCAF results show that the settling velocity of the lacustrine environment reaches the  
1030 434 peak of  $2.0 \text{ mm.s}^{-1}$  when SSC reach approximately  $2.0 \text{ g.L}^{-1}$ .

1031  
1032  
1033 435 In the estuary, the complex hydraulic regimes, including resuspension of freshly deposited  
1034 436 sediments (Marchesiello et al., 2019) and the mixing between fresh water and saline water led  
1035  
1036 437 to the formation of a zone of turbidity maximum and promote the formation of flocs (both  
1037  
1038 438 microflocs and macroflocs) (Dyer et al., 2002a and Manning et al., 2007). As a consequence,  
1039 439 the settling velocity also increases (Dyer et al., 2002b and Manning et al., 2011b). Beyond  $4.0$   
1040  
1041 440  $\text{g.L}^{-1}$ , hindered regime becomes predominant. It implies the decline of settling velocity in the

1045  
1046  
1047 441 lacustrine and estuarine environments, from 2.0 to 0.4 mm.s<sup>-1</sup> and from 0.8 to 0.1 mm.s<sup>-1</sup>,  
1048  
1049 442 respectively.  
1050  
1051 443 The main difference of these three environments is that flocculation processes seem to appear  
1052  
1053 444 at lower concentration in the fluvial environment (approximately 20 - 30 mg.L<sup>-1</sup>) than in the  
1054  
1055 445 lake (approximately 1 - 2 g.L<sup>-1</sup>) or in the estuary (approximately 300 mg.L<sup>-1</sup>). We cannot  
1056 446 exclude that the particles sampled in the fluvial environment are not real flocs, but correspond  
1057  
1058 447 to soil aggregates that are not in equilibrium with their hydraulic environment (Droppo et al.,  
1059  
1060 448 2005).  
1061  
1062 449 The flocculation efficiency is higher for the estuarine environment (+ 60 % of increase of the  
1063  
1064 450 settling velocity) and highest for lacustrine environment (+200 % of increase) than for the  
1065 451 fluvial environment (+7 % of increase).  
1066  
1067 452 Concerning the Flocculation Index (FI), sediment samples in the river and in the lake (red  
1068  
1069 453 circles for fluvial environment and yellow circles in lacustrine environment, see Fig. 5b)  
1070 454 exhibit a high dynamic, even in fresh water. The highest rate of flocculation is observed in the  
1071  
1072 455 lacustrine environment, where the measured FI increases from 0 to 6, when SSC increases  
1073  
1074 456 from 0.1 to 3.0 g.L<sup>-1</sup>. Interestingly, after getting the FI peak of 4 – 6, the efficiency of  
1075 457 flocculation in the lacustrine environment fell to value of 0 – 1.75. It means that flocculation  
1076  
1077 458 still occurs, but the volumetric concentration of particles is so high that the settling velocity  
1078 459 cannot increase anymore. Settling velocity of small particles is hindered by the high SSC,  
1079  
1080 460 whereas colloids are trapped on the surface of larger particles (Comba et al., 2009).  
1081  
1082 461 The estuarine sediments also experience three settling regimes with FI in range of 0 - 3: (1)  
1083  
1084 462 Free settling regime with constant FI of 2, that is developed at low concentration of 300 mg.L<sup>-1</sup>;  
1085  
1086 463 (2) Flocculation regime with FI < 3, where flocculation happens at SSC of 300 - 2700 mg.L<sup>-1</sup>;  
1087 464 (3) Hindered regime with FI of approximately 1 because of the appearance of brackish  
1088  
1089 465 water and high SSC of > 2.7 g.L<sup>-1</sup>. Flocs reach higher volumetric concentration for lower  
1090  
1091 466 mass concentrations when flocculation is reinforced by differential settling (Gratiot et al.,  
1092 467 2017).  
1093  
1094  
1095  
1096  
1097  
1098  
1099  
1100  
1101  
1102  
1103

1104  
1105  
1106  
1107  
1108  
1109  
1110  
1111  
1112  
1113  
1114  
1115  
1116  
1117  
1118  
1119  
1120  
1121  
1122  
1123  
1124  
1125  
1126  
1127  
1128  
1129  
1130  
1131  
1132  
1133  
1134  
1135  
1136  
1137  
1138  
1139  
1140  
1141  
1142  
1143  
1144



468 **Fig. 5.** Sediment properties in the Mekong Land to Ocean Continuum: (a) Variation of settling velocity with SSC measured directly with SCAF  
469 instrument and (b) Variation of the flocculation index with SSC.

## 4. Discussion

### 4.1. Suspended sediment transport mechanisms along the Mekong

As mentioned in Section 2.2.4, the transport regime of suspended sediment along the LMR may be characterized through the non-dimensional Rouse number ( $R_o$ ). For the upstream fluvial environment, the computed shear velocities were similar in the different sections monitored,  $u_* = 0.03 \text{ m.s}^{-1}$  for the MK10 and  $u_* = 0.04 \text{ m.s}^{-1}$  for MK16. The small difference between the two cross-sections may be explained by the geometry of each cross-section, MK10 cross-section being wider than MK16 cross-section. The shear velocity in the Tonle Sap is  $0.008 \text{ m.s}^{-1}$  by using SLIM simulation obtained by Le et al. (submitted); while a value of  $0.010 \text{ m.s}^{-1}$  is obtained by using the Inner law. The  $R_o$  values in the estuary are estimated based on two representative particle sizes ( $15 \mu\text{m}$  for fine particles and  $300 \mu\text{m}$  for sand) and the shear velocity is estimated with the recent work of Eidam et al. (2017).

The  $R_o$  values estimated for the fluvial, lacustrine and estuary environments are summarized in Table 1. In the fluvial environment, the  $R_o$  ranges between 0.002 and 0.009 at the two monitored river cross section (MK10 and MK16), which corresponds to the washload mode. Hence particles are presumably transported over long distances, without any interaction with the riverbed. Few sand particles are presents in the MK10 and MK16 cross section samples, with  $R_o$  values of 0.75 - 4.6. Its means that the very fine sand particles are strongly sorted over the water depth, leading to a low suspension mode. As for the coarser sand fraction of the riverbed, the stream was not able to transport them in suspension.

While  $R_o$  values of Tonle Sap samples vary from 0.005 – 0.015, corresponding to flow modes ranging from washload to strong suspension load (Vanoni et al., 1946 and Udo et al., 2011). It is assumed that sediments are deposited near bed during one part of the year, and eroded under wind-induced currents during another part of the year. According to Kummu (2008), the net budget of sediment is almost in equilibrium between deposition and erosion.

In the estuary, the value of the  $R_o$  for the fine sediments ranges between 0.007 - 0.058, which corresponds to strong suspension mode; while the values for sand vary from 2.4 to approximately 12, which corresponds to the bedload mode and sedimentation dominated regime (Gugliotta et al., 2019). This finding coincides with the recent study of Marchesiello et al. (2019) showing that the Mekong sediments consist of a mixture (fine sediments and sands)

under effects of complex forces. Thus coastal muds are exposed to wave-induced resuspension and wind-induced transport, while sands are concentrated near the estuaries.

**Table 1.** Ro value in two different conditions

Sample	Mean Diameter ( $\mu\text{m}$ )	$u_*$ ( $\text{m}\cdot\text{s}^{-1}$ )		$w_s$ ( $\text{m}\cdot\text{s}^{-1}$ )		Rouse value	
		Law of Wall	Modelled results	SCAF	Stokes' Law	Min	Max
Fluvial (MK10)	$19 \pm 2$	0.029	-	2.0E-05	1.2E-04	0.002	0.009
Fluvial (MK16)	$18 \pm 4$	0.041	-	8.0E-05	1.2E-04	0.005	0.007
Tonle Sap	$7 \pm 2$	0.014	0.008	5.0E-05	2.0E-05	0.005	0.015
Estuary fine sediment	$15 \pm 2$	-	0.01	3.0E-05	2.4E-04	0.007	0.058
Estuary sand	$300 \pm 30$	-	0.02	2.0E-02	9.5E-02	2.439	11.6

#### 4.2 Predominance of flocculi in the LMR and consequences for sediment transport

As quantified in this paper, flocculi is the dominant particles population in all three environments monitored at regional scale (46 % in the fluvial environment, 78 % in the lake and 78 % in the estuary). The existence of sand was noticed, but can mostly be found near the bed with few percent of volume.

In the Lower Mekong River as in many other large hydrosystems under tropical climates, we may anticipate that particles' populations (and its consequences) fluctuate seasonally and year after year. As designed, this study cannot catch these variations, however, we believe that it describes a general pattern that could be helpful when establishing some monitoring strategies in similar large tropical hydrosystems in South East Asia, and probably elsewhere. At large scale, Rouse analysis presented in Table 1 showed that particles are mainly transported with a strong suspension regime, evenly as washload by river flow. By these modes, they are transported abundantly along the main river and tributaries, partially over the floodplains during the flood season (Kondolf et al., 2014, Manh et al., 2014, Manh et al., 2015) and then, are deposited along shore and on the whole subaqueous delta, before having cycles of resuspension/deposition, principally under waves forcing (Marchesiello et al., 2019). Our measurements in the fluvial section show that few sands are transported in the water column because their transport, which do not flocculate, is completely governed by the stream power. During high flow with enhanced stream powers working with other sediment sources (riverbanks and floodplains), the finest sands are lifted into upper layer.

1263  
1264  
1265 523 This methodology can explain two distinct transport modes of two particles populations in the  
1266  
1267 524 Mekong estuary: washload is well mixed throughout the water column and sand are  
1268  
1269 525 transported prevailing near the bottom. It leads to distinct geomorphological forms, with the  
1270 526 presence of alternated tidal flats and sand bars as observed in many river mouths (Ta et al.,  
1271  
1272 527 2002; Gupta et al., 2002; Anthony, 2015).

#### 1274 528 *4.3. Occurrence of fluid mud layers in the Mekong estuary*

1275

1276  
1277 529 According to measured data during our three surveys in the estuary, a fluid mud layer was  
1278  
1279 530 sometimes formed near bottom, with SSC values abruptly increasing beyond  $0.4 \text{ g.L}^{-1}$ ,  
1280 531 corresponding to the transition to the flocculation regime (Fig. 5; Gratiot et al., 2017). Fig. 6  
1281  
1282 532 sketches the sediment transport from the river to the estuary in low flow season (a) and high  
1283 533 flow season (b) with locations of vertical profile sampling. In this figure, the blue profile  
1284  
1285 534 represents a schematic profile measured in low flow season and the purple one represents a  
1286 535 profile measured in high flow season. Fig. 7 reports all SSC value observed near bottom ( $z =$   
1287  
1288 536  $0.9h - SSC_{nb}$ ) for the vertical profiles realized in the estuary in December 2015 (50 profiles),  
1289  
1290 537 March 2016 (44 profiles) and October 2016 (47 profiles). Each vertical profile is represented  
1291 538 by a single point in Fig. 7. The three curves show the sorted distribution of all  $SSC_{nb}$  values  
1292  
1293 539 for the three seasons. The curves show that the percentage of profiles which exhibits high SSC  
1294 540 values, compatible with fluid mud layer occurrence, is very high during low flow season  
1295  
1296 541 (66 % of profiles in Dec 2015 and 95 % profiles in March 2016) and is much smaller during  
1297 542 high flow season (9 % profiles in October 2016).

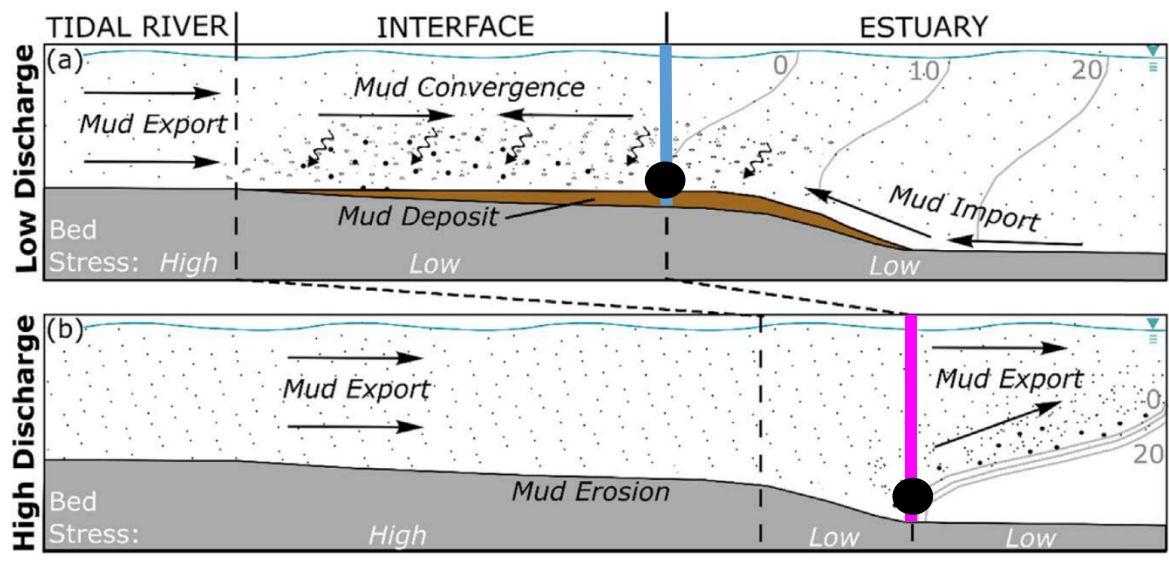
1298  
1299  
1300 543 By multiplying  $SSC_{nb}$  values with the corresponding settling velocity  $w_s$ , reported in Fig. 5, we  
1301  
1302 544 can estimate the settling flux capacity of fluid mud layers  $\phi = SSC_{nb} \times w_s$  and thus assess  
1303 545 their potential contribution to sedimentation (Fig. 7b). The cumulated sorted series  
1304  
1305 546 demonstrate the strong linearity between sediment concentration and settling flux (i.e.  
1306 547 potential of sedimentation). Fig.7c shows that the 10 % of the most concentrated fluid mud  
1307  
1308 548 layers contributes to 60 % of the sedimentation during low flow season (blue curves) and  
1309  
1310 549 more than 98 % during high flow season (purple curve).

1311  
1312 550 As a preliminary conclusion, our study confirms the existence of fluid mud layers and  
1313  
1314 551 quantifies broadly their frequency of occurrence in the estuary. Fluid mud layers are observed  
1315 552 within distances of approximately 30 km from the coastlines in both high flow and low flow  
1316  
1317 553 seasons. However according to Wolanski et al. (1998), the location of fluid mud layer in the  
1318  
1319  
1320  
1321



1322  
1323  
1324  
1325  
1326  
1327  
1328  
1329  
1330  
1331  
1332  
1333  
1334  
1335  
1336  
1337  
1338  
1339  
1340  
1341  
1342  
1343  
1344  
1345  
1346  
1347  
1348  
1349  
1350  
1351  
1352  
1353  
1354  
1355  
1356  
1357  
1358  
1359  
1360  
1361  
1362  
1363  
1364  
1365  
1366  
1367  
1368  
1369  
1370  
1371  
1372  
1373  
1374  
1375  
1376  
1377  
1378  
1379  
1380

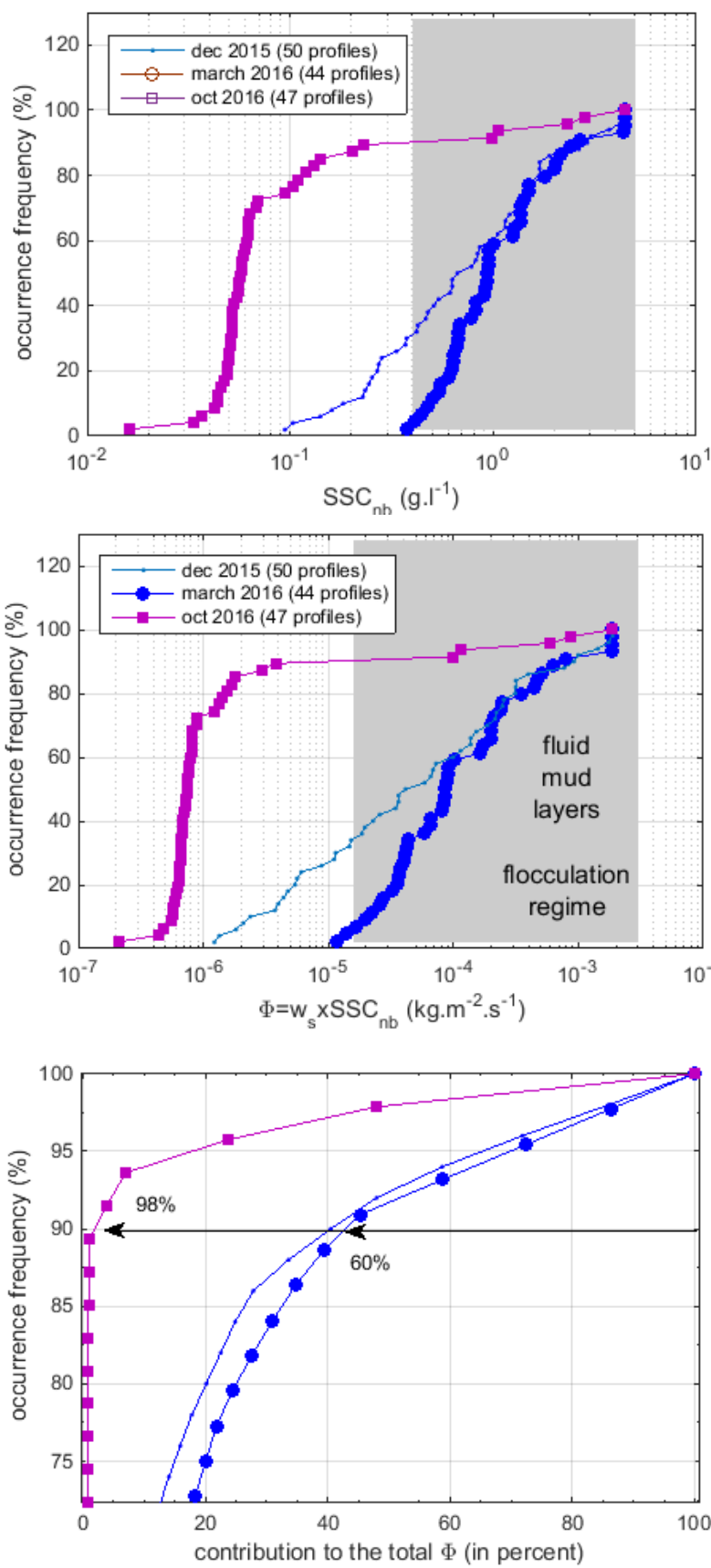
554 Mekong estuary varies spatially with river discharges and tides. In the high flow season, most  
555 of sediment deposits in shallow coastal waters, approximately 10 - 20 km from the coast  
556 (Wolanski et al., 1998 and Marchesiello et al., 2019). In low flow season, fine sediment is  
557 well mixed with saline water penetrating about 40 km inland, carrying sediment up-river to a  
558 turbidity maximum zone. Further upstream, at Can Tho, approximately 120 km from the  
559 coast, no turbidity maximum is found in the freshwater region of the estuary. Thus the  
560 positions of fluid mud layers and turbidity maximum, which are promoted by SSC  
561 concentration in the range 0.4 - 4 g.L<sup>-1</sup>, can hardly be observed for distances higher than 120  
562 km inland. This situation could change in the future, under the cumulated effect of subsidence  
563 and sea level rise.



564  
565 **Fig 6.** Conceptual summary of salinity stratification (grey lines), SSC (dot concentration),  
566 relative near-bed shear stress, suspended particle aggregation (dot size), net sediment  
567 advection (black arrows), and mud deposition/erosion within the tidal river, tidal river –  
568 estuary interface, and estuary during (a) low and (b) high discharge seasons. Relative weight  
569 of transport arrows vary with season and regime. Not drawn to scale (after McLachlan et al.,  
570 2017). The blue line shows the vertical profile in low flow season and the purple line shows  
571 one in high flow season with SSC. The black dot shows the sampling height (near bottom, at  
572 0.9 h).

573 According to Spearman and Manning (2008), the mass balance between accretion and erosion  
574 of cohesive sediment during tidal cycles in estuarial location can occur when threshold shear  
575 stresses for both deposition and erosion operate simultaneously.

1381  
 1382  
 1383  
 1384  
 1385  
 1386  
 1387  
 1388  
 1389  
 1390  
 1391  
 1392  
 1393  
 1394  
 1395  
 1396  
 1397  
 1398  
 1399  
 1400  
 1401  
 1402  
 1403  
 1404  
 1405  
 1406  
 1407  
 1408  
 1409  
 1410  
 1411  
 1412  
 1413  
 1414  
 1415  
 1416  
 1417  
 1418  
 1419  
 1420  
 1421  
 1422  
 1423  
 1424  
 1425  
 1426  
 1427  
 1428  
 1429  
 1430  
 1431  
 1432  
 1433  
 1434  
 1435  
 1436  
 1437  
 1438  
 1439



(a) **Fig 7.** Data corresponds to SSC measured near bottom ( $SSC_{nb}$ ). Data are sorted from lowest to highest SSC (a), corresponding settling flux (b) and contribution to the total (c). The blue line shows the vertical profile in December 2015; the blue line with dots shows one in March 2016 and the purple line shows one in October 2016 with SSC near bed.

(c)

1440  
1441  
1442 576 *4.4. Implication for Mekong Delta management*  
1443  
1444

1445 577 In the MD, the flocculation process plays an essential role in the formation of fluid mud layer  
1446 578 by enhancing the downward flux of sediment when freshwater mixes with seawater and  
1447 579 sediments become trapped at the convergence point. Sediments leaving the MD appears to go  
1448 580 through cycles of trapping and resuspension in the estuary, before being partially advected  
1449 581 seaward on the subaqueous delta and alongshelf, where they are largely incorporated into  
1450 582 fluid mud along the bottom salinity front. The fluid muds have far-reaching effects on the  
1451 583 coasts by reducing boundary shear stresses, attenuating of waves over a soft muddy bottom,  
1452 584 affecting water-column /seabed exchanges, and serving as the agent of outward growth of the  
1453 585 subaqueous delta (Marchesiello et al., 2019). In addition, fluid mud layers can lead to rise in  
1454 586 fluid viscosity and density, and the reduction of bottom shear stresses can affect on the tidal  
1455 587 wave propagation (Gabioux et al., 2005). Thus without flocculation, the particles would be  
1456 588 carried directly offshore (Kineke et al., 1996). The appearance of fluid mud layer under  
1457 589 flocculation regime provides a mechanism for rapid and strong sedimentation in the estuaries  
1458 590 and lead to local siltation and mud accretion. Once deposited in the bed, fluid mud layers  
1459 591 contribute to bedform development and stability (Schindler et al., 2015). We should underline  
1460 592 that bedform consolidation and stability is hardly predictable, because it depends on both  
1461 593 physical and biological near bed processes (Parson et al., 2016) that evolve continuously for  
1462 594 sediment mixtures containing cohesive mud and biologically active substances such as  
1463 595 microorganisms, bacteria and microphytobenthos who form biofilms (Malarkey et al., 2015).

1464 596 How can we anticipate the impact of human activities on sediment dynamics, flocculation and  
1465 597 fluid mud layer formation at regional scale? As reported in the recent publications of Schmitt  
1466 598 et al. (2017) and Thi Ha et al. (2018), human pressure, through sediment trapping and sand  
1467 599 mining, already leads to a significant decrease of SSC in the estuaries. Our study points out  
1468 600 that SSC is a determining factor affecting, first flocculation, and secondly, the formation of  
1469 601 fluid mud layers in the Mekong estuary. There is a critical treshold of around  $SSC = 0.4 \text{ g.L}^{-1}$ ,  
1470 602 that can be seen as a tipping point for sediment processes. If the occurrence of SSC beyond  
1471 603 that point decreases, the deposition rate will strongly reduce (no linear effects), while the  
1472 604 erosion rate will probably increase because of a decrease of sediment quantity, and because of  
1473 605 the reduction of drag coefficient in the regions of fluid muds (Dyer et al., 2002a), which  
1474 606 enhances boundary shear stresses nearshore, coinciding with erosional areas in the Mekong  
1475 607 estuaries (Kineke et al., 1996). As fluid mud layers in the Mekong estuaries are a key factor to

1499  
1500  
1501 608 promote flocculation and “boost” natural sedimentation, we do believe that some regular  
1502  
1503 609 monitoring programs should be realized. In terms of coastal management, a simple measure  
1504  
1505 610 that should be seriously considered is mangrove reforestation. Because of cohesiveness,  
1506  
1507 611 sediment particles transported out into mangrove forests during tidal inundation flocculate and  
1508  
1509 612 form larger flocs. Thus mangroves are not just passive colonisers of mud banks but they are  
1510  
1511 613 active in trapping suspended sediment, with positive feedback on shore protection (Furukawa  
1512  
1513 614 et al., 1997; Anthony and Gratiot, 2012; Gratiot and Anthony, 2016). This mechanism was  
1514  
1515 615 recently characterized through a deep geomorphological study conducted along the muddy  
1516  
1517 616 coast of the Guianas. In this environment, which is comparable to the Mekong shore, Brunier  
1518  
1519 617 et al. (2019) observed and quantified some exceptional rates of muddy shoreline retreat  
1520  
1521 618 following mangrove removal for field rice production. Apart from this mechanism, mangroves  
1522  
1523 619 play a role as a buffer between sea and land to prevent river sediment from re-entrainment to  
1524  
1525 620 the ocean at ebb tide (Furukawa and Wolanski, 1996).

## 1523 621 **5. Conclusions**

1524  
1525 622 Field surveys and laboratory analysis were performed at regional scale in the upper fluvial,  
1526  
1527 623 lacustrine and lower estuarine environments to provide a physically-based assessment of  
1528  
1529 624 sediment transport regimes, flocculation, and fluid mud layer dynamics along the Lower  
1530  
1531 625 Mekong River (LMR). The independent evaluation of particle size and settling velocity  
1532  
1533 626 provides a good assessment of particles behaviour, and allows characterizing the  $R_0$  number  
1534  
1535 627 and corresponding regimes in a robust way. Suspended sediments in fluvial and lacustrine  
1536  
1537 628 environments are predominantly flocculi (97 % and 100 % of total volume, respectively) and  
1538  
1539 629 primary particles, the modes are transported as washload or with a regime of strong  
1540  
1541 630 suspension. Some of these particles (primary particles and flocculi) probably experience  
1542  
1543 631 phases of deposition and resuspension, mostly in the adjacent floodplain, during their routing  
1544  
1545 632 through the Mekong basin, but we observed comparable sub distributions for fluvial,  
1546  
1547 633 lacustrine and even estuarine environments. This finding indicates that the primary particles  
1548  
1549 634 and flocculi populations very probably reach the estuary without any important physical  
1550  
1551 635 transformations (i.e. with similar PSD). In the estuary, the complex mixing between fluvial  
1552  
1553 636 and coastal waters and sediments offers optimal conditions of salinity, that leads to a higher  
1554  
1555 637 diversity of particles, with significant proportions of microflocs and macroflocs (25 % of total  
1556  
1557 638 volume), in the sand size range (diameter > 300  $\mu\text{m}$ ).

1558  
1559  
1560  
1561  
1562  
1563  
1564  
1565  
1566  
1567  
1568  
1569  
1570  
1571  
1572  
1573  
1574  
1575  
1576  
1577  
1578  
1579  
1580  
1581  
1582  
1583  
1584  
1585  
1586  
1587  
1588  
1589  
1590  
1591  
1592  
1593  
1594  
1595  
1596  
1597  
1598  
1599  
1600  
1601  
1602  
1603  
1604  
1605  
1606  
1607  
1608  
1609  
1610  
1611  
1612  
1613  
1614  
1615  
1616

639 The original estimation of flocculation indexes with SCAF instrument allows defining clearly  
640 the flocculation regime. This later is the most efficient for SSC in the range of 0.4 – 4 g.L<sup>-1</sup>. In  
641 fluvial, lacustrine and estuarine environments, flocculation regime develops for the same  
642 range of SSC, beyond ~0.4 g.L<sup>-1</sup>. Flocculation then becomes a key process, but its impacts on  
643 particles populations differs with the different environments. In the Tonle Sap lake,  
644 flocculation promotes the aggregation of colloids and primary particles on flocculi. In the  
645 estuarine environment, flocculation leads to the formation of a new population of particles, the  
646 micro-flocs. In the fluvial environment, the data were too scarce to draw a clear conclusion, as  
647 freshly eroded aggregates could not be yet in equilibrium with river hydro-sedimentary  
648 conditions.

649 As a consequence of these microscopic changes at scales of particles, our study confirms the  
650 regular occurrence of fluid mud layers (55 - 60% of occurrence) near bottom in the Mekong  
651 delta with distance of less than 120 km from the coastline, concentrated in 30 km in both high  
652 - and low - flow seasons. Fluid mud layers, which are intrinsically linked with flocculation  
653 processes, are early steps of landforms evolutions and participate to the geomorphology of the  
654 Mekong Delta (MD). In the light of this study and considering the degree of vulnerability of  
655 the delta to ongoing hydro-sedimentary changes, we may provide two recommendations:  
656 Firstly, the continental sediment flux needs to be restored (or at least maintained) and human  
657 driven subsidence needs to be controlled. Under those conditions, fluid mud layers should  
658 remain a driver of river and coastal geomorphology, as it has been the case over the last  
659 millennia. Secondly, the perception of mangrove should be reconsidered as reforestation is  
660 probably the optimal manner, in both technical and environmental aspects, for ensuring  
661 sediment trapping and preserving fluid mud layers and mudflat, with positive feedbacks on  
662 mangrove colonization. In other words, mangroves cannot compensate regional  
663 disequilibrium in sediment balance, but they can facilitate the transformation of diluted  
664 suspended sediment into fluid mud layers.

665 Taking into account the degree of uncertainty of field and laboratory measurements with  
666 natural fresh sediments, and the degree of variability of sediment properties in such large and  
667 human-impacted systems, there is a clear interest to adopt a monitoring strategy that would  
668 extend the study in time and space.

669

1617  
1618  
1619  
1620  
1621  
1622  
1623  
1624  
1625  
1626  
1627  
1628  
1629  
1630  
1631  
1632  
1633  
1634  
1635  
1636  
1637  
1638  
1639  
1640  
1641  
1642  
1643  
1644  
1645  
1646  
1647  
1648  
1649  
1650  
1651  
1652  
1653  
1654  
1655  
1656  
1657  
1658  
1659  
1660  
1661  
1662  
1663  
1664  
1665  
1666  
1667  
1668  
1669  
1670  
1671  
1672  
1673  
1674  
1675

670 **Acknowledgements**

671 The authors would like to thank the Université catholique de Louvain, Belgium for Hoang-  
672 Anh Le's doctoral fellowship, the Institut de Recherche pour le Développement (IRD -  
673 France) to support the field surveys in Laos and in Vietnam with the financial support of  
674 the Lower Mekong Delta coastal zones project (<http://lmdcz.siwrr.org.vn>). We also would like  
675 to thanks VolTransMESKONG CNES/TOSCA project to support the monitoring in Cambodia  
676 with the technical and scientific support of staff from LOG UMR8187 and the Institute of  
677 Technology of Cambodia, especially.

678 **References**

679 1. Anthony, E. J., & Gratiot, N. (2012). Coastal engineering and large-scale mangrove  
680 destruction in Guyana, South America: Averting an environmental catastrophe in the  
681 making. *Ecological Engineering*, 47, 268-273.

682 2. Anthony, E.J., (2015). Wave influence in the construction, shaping and destruction of river  
683 deltas: A review. *Marine Geology*, 361, 53-78.

684 3. Antoine, G., Cazilhac, M., Monnoyer, Q., Jodeau, M., Gratiot, N., Besnier, A. L., ... & Le  
685 Brun, M. (2015, April). Lateral and vertical heterogeneity of flow and suspended sediment  
686 characteristics during a dam flushing event, in high velocity conditions. In *EGU General  
687 Assembly Conference Abstracts (Vol. 17)*.

688 4. Azhikodan, G., & Yokoyama, K. (2018). Sediment transport and fluid mud layer formation  
689 in the macro-tidal Chikugo river estuary during a fortnightly tidal cycle. *Estuarine, Coastal  
690 and Shelf Science*, 202, 232-245.

691 5. Azrulhisham, E. A., & Azri, M. A. (2018, February). Application of LISST instrument for  
692 suspended sediment and erosive wear prediction in run-of-river hydropower plants.  
693 In *2018 IEEE International Conference on Industrial Technology (ICIT)* (pp. 886-891).  
694 IEEE.

695 6. Bachmann, R. W., Hoyer, M. V., Vinzon, S. B., & Daniel Jr, E. C. (2005). The origin of  
696 the fluid mud layer in Lake Apopka, Florida. *Limnology and Oceanography*, 50(2), 629-  
697 635.

698 7. Balica, S., Dinh, Q., Popescu, I., Vo, T. Q., & Pham, D. Q. (2014). Flood impact in the  
699 Mekong delta, Vietnam. *Journal of Maps*, 10(2), 257-268.

1676  
1677  
1678  
1679  
1680  
1681  
1682  
1683  
1684  
1685  
1686  
1687  
1688  
1689  
1690  
1691  
1692  
1693  
1694  
1695  
1696  
1697  
1698  
1699  
1700  
1701  
1702  
1703  
1704  
1705  
1706  
1707  
1708  
1709  
1710  
1711  
1712  
1713  
1714  
1715  
1716  
1717  
1718  
1719  
1720  
1721  
1722  
1723  
1724  
1725  
1726  
1727  
1728  
1729  
1730  
1731  
1732  
1733  
1734

700 8. Brunier, G., Anthony, E. J., Gratiot, N., & Gardel, A. (2019). Exceptional rates and  
701 mechanisms of muddy shoreline retreat following mangrove removal. *Earth Surface*  
702 *Processes and Landforms*.

703 9. Camenen, B., & van Bang, D. P. (2011). Modelling the settling of suspended sediments for  
704 concentrations close to the gelling concentration. *Continental Shelf Research*, 31(10),  
705 S106-S116.

706 10. Camenen, B., Le Coz, J., Dramais, G., Peteuil, C., Fretaud, T., Falgon, A., ... & Moore, S.  
707 A. (2014). A simple physically-based model for predicting sand transport dynamics in the  
708 Lower Mekong River. In *Proc. River Flow conference*, Lausanne, Switzerland, 8p.

709 11. Castro-Orgaz, O., Giráldez, J. V., Mateos, L., & Dey, S. (2012). Is the von Kármán  
710 constant affected by sediment suspension?. *Journal of Geophysical Research: Earth*  
711 *Surface*, 117(F4).

712 12. Comba, S., & Sethi, R. (2009). Stabilization of highly concentrated suspensions of iron  
713 nanoparticles using shear-thinning gels of xanthan gum. *Water Research*, 43(15), 3717-  
714 3726.

715 13. Darby, S. E., Hackney, C. R., Leyland, J., Kumm, M., Lauri, H., Parsons, D. R., ... &  
716 Aalto, R. (2016). Fluvial sediment supply to a mega-delta reduced by shifting tropical-  
717 cyclone activity. *Nature*, 539(7628), 276.

718 14. Droppo, I. G., Nackaerts, K., Walling, D. E., & Williams, N. (2005). Can flocs and water  
719 stable soil aggregates be differentiated within fluvial systems?. *Catena*, 60(1), 1-18.

720 15. Dyer, K. R., Bale, A. J., Christie, M. C., Feates, N., Jones, S., & Manning, A. J. (2002).  
721 The turbidity maximum in a mesotidal estuary, the Tamar Estuary, UK: I. Dynamics of  
722 suspended sediment. In *Proceedings in Marine Science* (Vol. 5, pp. 203-218). Elsevier.

723 16. Dyer, K. R., Bale, A. J., Christie, M. C., Feates, N., Jones, S., & Manning, A. J. (2002b).  
724 The turbidity maximum in a mesotidal estuary, the Tamar estuary, UK: II. The flocculation  
725 properties. In *Proceedings in Marine Science* (Vol. 5, pp. 219-232). Elsevier.

726 17. Edmonds, D. A., & Slingerland, R. L. (2010). Significant effect of sediment cohesion on  
727 delta morphology. *Nature Geoscience*, 3(2), 105.

728 18. Eidam, E. F., Nittrover, C. A., Ogston, A. S., DeMaster, D. J., Liu, J. P., Nguyen, T. T., &  
729 Nguyen, T. N. (2017). Dynamic controls on shallow clinoform geometry: Mekong Delta,  
730 Vietnam. *Continental Shelf Research*, 147, 165-181.

731 19. Farrell, E. J., & Sherman, D. J. (2013). Estimates of the Schmidt Number for vertical flux  
732 distributions of wind-blown sand. *Journal of Coastal Research*, 65(sp2), 1289-1295.

1735  
1736  
1737  
1738  
1739  
1740  
1741  
1742  
1743  
1744  
1745  
1746  
1747  
1748  
1749  
1750  
1751  
1752  
1753  
1754  
1755  
1756  
1757  
1758  
1759  
1760  
1761  
1762  
1763  
1764  
1765  
1766  
1767  
1768  
1769  
1770  
1771  
1772  
1773  
1774  
1775  
1776  
1777  
1778  
1779  
1780  
1781  
1782  
1783  
1784  
1785  
1786  
1787  
1788  
1789  
1790  
1791  
1792  
1793

- 733 20. Fennessy, M. J., Dyer, K. R., & Huntley, D. A. (1994). Size and settling velocity  
734 distributions of flocs in the Tamar Estuary during a tidal cycle. *Netherland Journal of*  
735 *Aquatic Ecology*, 28(3-4), 275-282.
- 736 21. Fettweis, M., Francken, F., Pison, V., & Van den Eynde, D. (2006). Suspended particulate  
737 matter dynamics and aggregate sizes in a high turbidity area. *Marine Geology*, 235(1-4),  
738 63-74.
- 739 22. Furukawa, K., & Wolanski, E. (1996). Sedimentation in mangrove forests. *Mangroves and*  
740 *Salt Marshes*, 1(1), 3-10.
- 741 23. Furukawa, K., Wolanski, E., & Mueller, H. (1997). Currents and sediment transport in  
742 mangrove forests. *Estuarine, Coastal and Shelf Science*, 44(3), 301-310.
- 743 24. Gabioux, M., Vinzon, S. B., & Paiva, A. M. (2005). Tidal propagation over fluid mud  
744 layers on the Amazon shelf. *Continental Shelf Research*, 25(1), 113-125.
- 745 25. Gratiot, N., Gardel, A. and Anthony, E.J., 2007. Trade-wind waves and mud dynamics on  
746 the French Guiana coast, South America: input from ERA-40 wave data and field  
747 investigations. *Marine Geology*. 236, 15-26.
- 748 26. Gratiot, N., Coulaud, C., Legout, C., Mercier, B., Mora, H., & Wendling, V. (2015). Unit  
749 for measuring the falling speed of particles in suspension in a fluid and device comprising  
750 at least one measuring unit and one automatic sampler. Patent - Publication number  
751 WO2015055963 A, 1.
- 752 27. Gratiot, N., & Anthony, E. J. (2016). Role of flocculation and settling processes in  
753 development of the mangrove-colonized, Amazon-influenced mud-bank coast of South  
754 America. *Marine Geology*, 373, 1-10.
- 755 28. Gratiot, N., Bildstein, A., Anh, T. T., Thoss, H., Denis, H., Michallet, H., & Apel, H.  
756 (2017). Sediment flocculation in the Mekong River estuary, Vietnam, an important driver  
757 of geomorphological changes. *Comptes Rendus Geoscience*, 349(6-7), 260-268.
- 758 29. Gugliotta, M., Saito, Y., Nguyen, V. L., Ta, T. K. O., & Tamura, T. (2019). Sediment  
759 distribution and depositional processes along the fluvial to marine transition zone of the  
760 Mekong River delta, Vietnam. *Sedimentology*, 66(1), 146-164.
- 761 30. Gupta, A., & Liew, S. C. (2007). The Mekong from satellite imagery: A quick look at a  
762 large river. *Geomorphology*, 85(3-4), 259-274.
- 763 31. Hai, P. T., Masumoto, T., & Shimizu, K. (2008). Development of a two-dimensional finite  
764 element model for inundation processes in the Tonle Sap and its environs. *Hydrological*  
765 *Processes: An International Journal*, 22(9), 1329-1336.



1794  
1795  
1796  
1797  
1798  
1799  
1800  
1801  
1802  
1803  
1804  
1805  
1806  
1807  
1808  
1809  
1810  
1811  
1812  
1813  
1814  
1815  
1816  
1817  
1818  
1819  
1820  
1821  
1822  
1823  
1824  
1825  
1826  
1827  
1828  
1829  
1830  
1831  
1832  
1833  
1834  
1835  
1836  
1837  
1838  
1839  
1840  
1841  
1842  
1843  
1844  
1845  
1846  
1847  
1848  
1849  
1850  
1851  
1852

- 766 32. Hung, N. N., Delgado, J. M., Güntner, A., Merz, B., Bárdossy, A., & Apel, H. (2014).  
767 Sedimentation in the floodplains of the Mekong Delta, Vietnam Part II: deposition and  
768 erosion. *Hydrological Processes*, 28(7), 3145-3160.
- 769 33. Kineke, G. C., Sternberg, R. W., Trowbridge, J. H., & Geyer, W. R. (1996). Fluid-mud  
770 processes on the Amazon continental shelf. *Continental Shelf Research*, 16(5-6), 667-696.
- 771 34. Kondolf, G. M., Rubin, Z. K., & Minear, J. T. (2014). Dams on the Mekong: Cumulative  
772 sediment starvation. *Water Resources Research*, 50(6), 5158-5169.
- 773 35. Kummu, M., & Sarkkula, J. (2008). Impact of the Mekong River flow alteration on the  
774 Tonle Sap flood pulse. *AMBIO: AMBIO*, 37(3), 185-193.
- 775 36. Kummu M, Tes S, Yin S, Adamson P, Jozsa J, Koponen J, Richey J, Sarkkula J (2014)  
776 Water balance analysis for the Tonle Sap Lake - floodplain system. *Hydrological*  
777 *Processes* 28(4):1722-1733.
- 778 37. Le, H. A., Lambrechts, J., Ortled, S., Gratiot, N., Deleersnijder, E., Soares-Fraza, S.,  
779 (2019). An implicit wetting - drying algorithm for the Discontinuous Galerkin method:  
780 Application to the Tonle Sap, Mekong River Basin. *Environmental Fluid Mechanics* (in  
781 submission).
- 782 38. Lee, B. J., Fettweis, M., Toorman, E., & Molz, F. J. (2012). Multimodality of a particle  
783 size distribution of cohesive suspended particulate matters in a coastal zone. *Journal of*  
784 *Geophysical Research: Oceans*, 117(C3).
- 785 39. Malarkey, J., Baas, J. H., Hope, J. A., Aspden, R. J., Parsons, D. R., Peakall, J., ... & Bass,  
786 S. J. (2015). The pervasive role of biological cohesion in bedform development. *Nature*  
787 *communications*, 6, 6257.
- 788 40. Manh, N.V., Dung, N.V., Hung, N.N., Merz, B., & Apel, H. (2014). Large-scale  
789 quantification of suspended sediment transport and deposition in the Mekong  
790 Delta. *Hydrology and Earth System Sciences Discussions*, 11(4).
- 791 41. Manh, N.V, Dung, N. V., Hung, N. N., Kummu, M., Merz, B., & Apel, H. (2015). Future  
792 sediment dynamics in the Mekong Delta floodplains: Impacts of hydropower  
793 development, climate change and sea level rise. *Global and Planetary Change*, 127, 22-33.
- 794 42. Manning, A. J., Friend, P. L., Prowse, N., & Amos, C. L. (2007). Estuarine mud  
795 flocculation properties determined using an annular mini-flume and the LabSFLOC  
796 system. *Continental Shelf Research*, 27(8), 1080-1095.
- 797 43. Manning, A. J., Baugh, J. V., Spearman, J. R., & Whitehouse, R. J. (2010). Flocculation  
798 settling characteristics of mud: sand mixtures. *Ocean dynamics*, 60(2), 237-253.

1853  
1854  
1855  
1856  
1857  
1858  
1859  
1860  
1861  
1862  
1863  
1864  
1865  
1866  
1867  
1868  
1869  
1870  
1871  
1872  
1873  
1874  
1875  
1876  
1877  
1878  
1879  
1880  
1881  
1882  
1883  
1884  
1885  
1886  
1887  
1888  
1889  
1890  
1891  
1892  
1893  
1894  
1895  
1896  
1897  
1898  
1899  
1900  
1901  
1902  
1903  
1904  
1905  
1906  
1907  
1908  
1909  
1910  
1911

- 799 44. Manning, A.J., Baugh, J.V., Soulsby, R.L., Spearman, J.R., Whitehouse, R.J.S., 2011a.  
800 Cohesive sediment flocculation and the application to settling flux modelling (Chapter 5).  
801 In: Ginsberg, Silvia Susana (Ed.), Sediment Transport. InTech, Vienna, ISBN: 978-953-  
802 307-189-3, pp. 91–116.
- 803 45. Manning, A. J., Baugh, J. V., Spearman, J. R., Pidduck, E. L., & Whitehouse, R. J.  
804 (2011b). The settling dynamics of flocculating mud-sand mixtures: Part 1—Empirical  
805 algorithm development. *Ocean Dynamics*, 61(2-3), 311-350.
- 806 46. Marchesiello, P., Nguyen, N.M., Gratiot, N., Loisel, H., Anthony, E.J. and Nguyen, T.,  
807 2019. Erosion of the coastal Mekong delta: Assessing natural against man induced  
808 processes. *Continental Shelf Research*, 181, 72-89.
- 809 47. McAnally, W. H., Friedrichs, C., Hamilton, D., Hayter, E., Shrestha, P., Rodriguez, H., ...  
810 & ASCE Task Committee on Management of Fluid Mud. (2007). Management of fluid  
811 mud in estuaries, bays, and lakes. I: Present state of understanding on character and  
812 behavior. *Journal of Hydraulic Engineering*, 133(1), 9-22.
- 813 48. McLachlan, R. L., Ogston, A. S., & Allison, M. A. (2017). Implications of tidally - varying  
814 bed stress and intermittent estuarine stratification on fine-sediment dynamics through the  
815 Mekong's tidal river to estuarine reach. *Continental Shelf Research*, 147, 27-37.
- 816 49. Mehta, A. J. (1991). Understanding fluid mud in a dynamic environment. *Geo-Marine*  
817 *Letters*, 11(3-4), 113-118.
- 818 50. Mekong River Commission portal, available at <http://www.mrcmekong.org/>.
- 819 51. Mikkelsen, O. A., Hill, P. S., & Milligan, T. G. (2006). Single-grain, microfloc and  
820 macrofloc volume variations observed with a LISST-100 and a digital floc  
821 camera. *Journal of Sea Research*, 55(2), 87-102.
- 822 52. Milliman, J. D., & Meade, R. H. (1983). World-wide delivery of river sediment to the  
823 oceans. *The Journal of Geology*, 91(1), 1-21.
- 824 53. Nguyen, T. T., Némery, J., Gratiot, N., Garnier, J., Strady, E., Tran, V. Q., ... & Aimé, J.  
825 (2019). Phosphorus adsorption/desorption processes in the tropical Saigon River estuary  
826 (Southern Vietnam) impacted by a megacity. *Estuarine, Coastal and Shelf Science*,  
827 106321.
- 828 54. Nittrouer, C. A., DeMaster, D. J., Eidam, E. F., Nguyen, T. T., Liu, J. P., Ogston, A. S., &  
829 Phung, P. V. (2017). The Mekong continental shelf: The primary sink for deltaic sediment  
830 particles and their passengers. *Oceanography*, 30(3), 60-70.

1912  
1913  
1914  
1915  
1916  
1917  
1918  
1919  
1920  
1921  
1922  
1923  
1924  
1925  
1926  
1927  
1928  
1929  
1930  
1931  
1932  
1933  
1934  
1935  
1936  
1937  
1938  
1939  
1940  
1941  
1942  
1943  
1944  
1945  
1946  
1947  
1948  
1949  
1950  
1951  
1952  
1953  
1954  
1955  
1956  
1957  
1958  
1959  
1960  
1961  
1962  
1963  
1964  
1965  
1966  
1967  
1968  
1969  
1970

- 831 55. Nowacki, D. J., Ogston, A. S., Nittrouer, C. A., Fricke, A. T., & Van, P. D. T. (2015).  
832 Sediment dynamics in the lower Mekong River: Transition from tidal river to  
833 estuary. *Journal of Geophysical Research: Oceans*, 120(9), 6363-6383.
- 834 56. Parsons, D. R., Schindler, R. J., Hope, J. A., Malarkey, J., Baas, J. H., Peakall, J., ... &  
835 Aspden, R. J. (2016). The role of biophysical cohesion on subaqueous bed form  
836 size. *Geophysical research letters*, 43(4), 1566-1573.
- 837 57. Peteuil, C., Frétau, T., Wirz, C., Camenen, B., Guertault, L., Le Coz, J., & Dramais, G.  
838 (2014). Importance of field observation for managing sediment fluxes in hydropower  
839 projects design and operation. In *Proceedings of the 19th IAHR-APD Congress, Hanoi,*  
840 *Vietnam.*
- 841 58. Ribolzi, O., Evrard, O., Huon, S., Rouw, A. De, Silvera, N., Latschack, O., Soulileuth, B.,  
842 Lefèvre, I., Pierret, A., 2017. From shifting cultivation to teak plantation: effect on  
843 overland flow and sediment yield in a montane tropical catchment. *Sci. Rep.* 1–12.
- 844 59. Rijn, L. C. V. (1984). Sediment transport, part II: suspended load transport. *Journal of*  
845 *Hydraulic Engineering*, 110(11), 1613-1641.
- 846 60. Rouse, H. (1937). Modern conceptions of the mechanics of fluid turbulence. *Trans*  
847 *ASCE*, 102, 463-505.
- 848 61. Santini, W., Camenen, B., Coz, J. L., Vauchel, P., Guyot, J. L., Lavado, W., ... & Espinoza  
849 Villar, R. (2019). An index concentration method for suspended load monitoring in large  
850 rivers of the Amazonian foreland. *Earth Surface Dynamics*, 7(2), 515-536.
- 851 62. Schindler, R. J., Parsons, D. R., Ye, L., Hope, J. A., Baas, J. H., Peakall, J., ... & Paterson,  
852 D. M. (2015). Sticky stuff: Redefining bedform prediction in modern and ancient  
853 environments. *Geology*, 43(5), 399-402.
- 854 63. Schmitt, R. J. P., Rubin, Z., & Kondolf, G. M. (2017). Losing ground-scenarios of land  
855 loss as consequence of shifting sediment budgets in the Mekong  
856 Delta. *Geomorphology*, 294, 58-69.
- 857 64. Schelske, C. L. (2006). Comment on the origin of the “fluid mud layer” in Lake Apopka,  
858 Florida. *Limnology and Oceanography*, 51(5), 2472-2480.
- 859 65. Seah, K. C., Qasim, G. H., Hong, Y. S., Kim, E., Kim, K. T., & Han, S. (2017).  
860 Assessment of colloidal copper speciation in the Mekong River Delta using diffusive  
861 gradients in thin film techniques. *Estuarine, Coastal and Shelf Science*, 188, 109-115.
- 862 66. Sequioia. LISST-Portable|XR User's Manual Version 1.2 (2016).
- 863 67. Siev S, Paringit EC, Yoshimura C, Hul S (2016) Seasonal Changes in the Inundation Area  
864 and Water Volume of the Tonle Sap River and Its Floodplain. *Hydrology* 3(4):33-45.

1971  
1972  
1973  
1974  
1975  
1976  
1977  
1978  
1979  
1980  
1981  
1982  
1983  
1984  
1985  
1986  
1987  
1988  
1989  
1990  
1991  
1992  
1993  
1994  
1995  
1996  
1997  
1998  
1999  
2000  
2001  
2002  
2003  
2004  
2005  
2006  
2007  
2008  
2009  
2010  
2011  
2012  
2013  
2014  
2015  
2016  
2017  
2018  
2019  
2020  
2021  
2022  
2023  
2024  
2025  
2026  
2027  
2028  
2029

865 68. Sim, S. Y., Chan, D. C. H., Huang, T. F., Chai, W., Isaacson, T., Flood Jr, J. C., ... &  
866 Orzen, M. (2007). U.S. Patent No. 7,272,613. Washington, DC: U.S. Patent and  
867 Trademark Office.

868 69. Sime, L. C., Ferguson, R. I., & Church, M. (2007). Estimating shear stress from moving  
869 boat acoustic Doppler velocity measurements in a large gravel bed river. *Water Resources*  
870 *Research*, 43(3).

871 70. Smardon, R. (2009). Restoration of the Tram Chim National Wildlife Preserve, Vietnam.  
872 *Sustaining the World's Wetlands*, 153–178.

873 71. Sottolichio, A., Hurther, D., Gratiot, N., Bretel, P., 2011. Acoustic turbulence  
874 measurements of near-bed suspended sediment dynamics in highly turbid waters of a  
875 macrotidal estuary. *Continental Shelf Research*, 31, S36-S49.

876 72. Spearman, J., & Manning, A. J. (2008). On the significance of mud transport algorithms  
877 for the modelling of intertidal flats. In *Proceedings in Marine Science* (Vol. 9, pp. 411-  
878 430). Elsevier.

879 73. Stokes, G. G. (1857). On the effect of wind on the intensity of sound. *Brit. Assoc.*  
880 *Report*, 22.

881 74. Ta, T. K. O., Nguyen, V. L., Tateishi, M., Kobayashi, I., Tanabe, S., & Saito, Y. (2002).  
882 Holocene delta evolution and sediment discharge of the Mekong River, southern  
883 Vietnam. *Quaternary Science Reviews*, 21(16-17), 1807-1819.

884 75. Thi Ha, D., Ouillon, S., & Van Vinh, G. (2018). Water and suspended sediment budgets in  
885 the lower Mekong from high-frequency measurements (2009–2016). *Water*, 10(7), 846.

886 76. Toorman, E.A., Anthony, E., Augustinus, P.G.E.F., Gardel, A., Gratiot, N., Homenauth,  
887 O., Huybrechts, N., Monbaliu, J., Moseley, K., Naipal, S. 2018. Interaction of mangroves,  
888 coastal hydrodynamics and morphodynamics along the coastal fringes of the Guianas.  
889 *Coastal research library series*, Springer book, pp 429-473.

890 77. Tran, D. D., Van Halsema, G., Hellegers, P. J., Hoang, L. P., Tran, T. Q., Kumm, M., &  
891 Ludwig, F. (2018). Assessing impacts of dike construction on the flood dynamics of the  
892 Mekong Delta. *Hydrology and Earth System Sciences*, 22(3).

893 78. Tri, V. K. (2012). Hydrology and hydraulic infrastructure systems in the Mekong Delta,  
894 Vietnam. In *The Mekong Delta System* (pp. 49-81). Springer, Dordrecht.

895 79. Udo, K., & Mano, A. (2011). Application of Rouse's Sediment Concentration Profile to  
896 Aeolian Transport: Is the suspension system for sand transport in air the same as that in  
897 water?. *Journal of Coastal Research*, 2079-2083.

2030  
2031  
2032  
2033  
2034  
2035  
2036  
2037  
2038  
2039  
2040  
2041  
2042  
2043  
2044  
2045  
2046  
2047  
2048  
2049  
2050  
2051  
2052  
2053  
2054  
2055  
2056  
2057  
2058  
2059  
2060  
2061  
2062  
2063  
2064  
2065  
2066  
2067  
2068  
2069  
2070  
2071  
2072  
2073  
2074  
2075  
2076  
2077  
2078  
2079  
2080  
2081  
2082  
2083  
2084  
2085  
2086  
2087  
2088

- 898 80. Uncles, R. J., Stephens, J. A., & Law, D. J. (2006). Turbidity maximum in the macrotidal,  
899 highly turbid Humber Estuary, UK: Flocs, fluid mud, stationary suspensions and tidal  
900 bores. *Estuarine, Coastal and Shelf Science*, 67(1-2), 30-52.
- 901 81. Van, L. A., & Van Bang, D. P. (2013). Hindered settling of sand–mud flocs mixtures:  
902 From model formulation to numerical validation. *Advances in Water Resources*, 53, 1-11.
- 903 82. Van Leussen, 1994. Estuarine macroflocs and their role in fine-grained sediment  
904 transport. Ph.D. thesis, University of Utrecht, The Netherlands.
- 905 83. Vanoni, V. A. (1946). Transportation of suspended sediment by water. *Trans. of*  
906 *ASCE*, 111, 67-102.
- 907 84. W.C. Rouse. U.S. Patent and Trademark Office (1938).
- 908 85. Wendling, V., Gratiot, N., Legout, C., Droppo, I. G., Coulaud, C., & Mercier, B. (2015).  
909 Using an optical settling column to assess suspension characteristics within the free,  
910 flocculation, and hindered settling regimes. *Journal of Soils and Sediments*, 15(9), 1991-  
911 2003.
- 912 86. Windt, C., Ebrahimian, A., & Traver, R. Flow Characterization of Stormwater Runoff in  
913 Philadelphia. In *World Environmental and Water Resources Congress 2017* (pp. 365-371).
- 914 87. Winterwerp, J. C. (2002). On the flocculation and settling velocity of estuarine  
915 mud. *Continental Shelf Research*, 22(9), 1339-1360.
- 916 88. Winterwerp, J. C. (2011). Fine sediment transport by tidal asymmetry in the high-  
917 concentrated Ems River: indications for a regime shift in response to channel  
918 deepening. *Ocean Dynamics*, 61(2-3), 203-215.
- 919 89. Wolanski, E., Huan, N. N., Nhan, N. H., & Thuy, N. N. (1996). Fine-sediment dynamics in  
920 the Mekong River estuary, Vietnam. *Estuarine, Coastal and Shelf Science*, 43(5), 565-582.
- 921 90. Wolanski, E., Nhan, N. H., & Spagnol, S. (1998). Sediment dynamics during low flow  
922 conditions in the Mekong River estuary, Vietnam. *Journal of Coastal Research*, 472-482.
- 923 91. Xing, F., Meselhe, E. A., Allison, M. A., & Weathers III, H. D. (2017). Analysis and  
924 numerical modeling of the flow and sand dynamics in the lower Song Hau channel,  
925 Mekong Delta. *Continental Shelf Research*, 147, 62-77.

2089  
2090  
2091  
2092  
2093  
2094  
2095  
2096  
2097  
2098  
2099  
2100  
2101  
2102  
2103  
2104  
2105  
2106  
2107  
2108  
2109  
2110  
2111  
2112  
2113  
2114  
2115  
2116  
2117  
2118  
2119  
2120  
2121  
2122  
2123  
2124  
2125  
2126  
2127  
2128  
2129  
2130  
2131  
2132  
2133  
2134  
2135  
2136  
2137  
2138  
2139  
2140  
2141  
2142  
2143  
2144  
2145  
2146  
2147

926

## Appendix

927 Fig. a, b, c display the detailed PSD for some representative samples collected in fluvial,  
 928 lacustrine and estuarine environments, respectively. For clarity purposes, only a limited (nine)  
 929 number of samples are represented in the first panel row. The second row exhibits  
 930 representative PSDs without sonication and the last row is for representative PSDs with  
 931 sonication. After two minutes of sonication, all three environments show higher percentages  
 932 of smallest constituents, namely primary particles. The mean size of samples taken in the  
 933 fluvial and lacustrine parts is smaller than ones taken in the estuary, especially after  
 934 sonication, a considerable constituent of primary particles is found in the upper parts. In  
 935 addition, the particle size in Tonle Sap was smallest, with mean diameter of approximately 7  
 936  $\mu\text{m}$  and primary particles are predominance. In contrast, the graphs illustrate the large  
 937 variation of particle sizes in the delta, predominantly in range of 10 - 386  $\mu\text{m}$  before  
 938 sonication and 2.21 - 331  $\mu\text{m}$  after sonication. It is clear that sand appears in the Mekong  
 939 estuary with percentage of 11 %; a median diameter of  $> 300 \mu\text{m}$ .

### (a) Fluvial

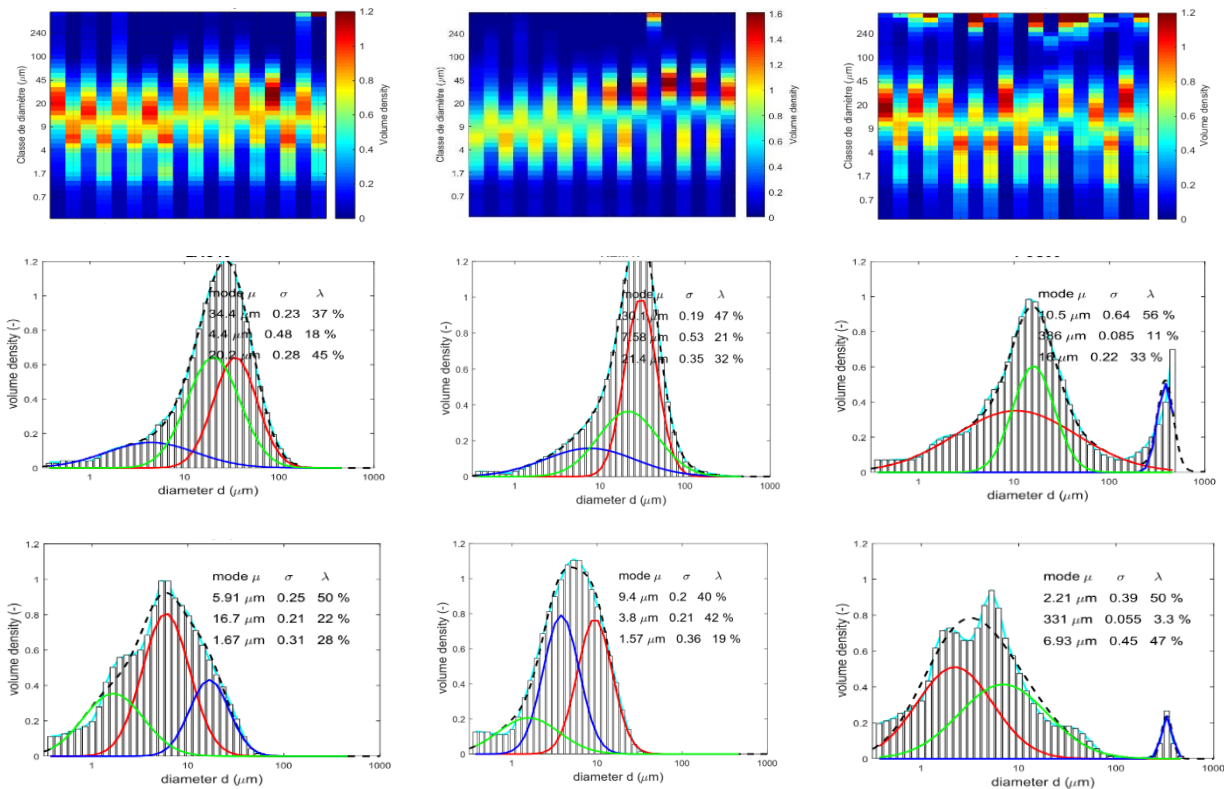
### (b) Lacustrine

### (c) Estuarine

Mekong river, Laos, 06/2017

Tonle Sap, Cambodia,  
09/2018

Mekong estuary, Vietnam,  
03/2016



940 **Fig.** PSD of three representative samples in fluvial, lacustrine and estuarine environments

Conflict of interests :

On behalf of co-authors, I declare no conflict of interests.